Summer 2013

Analysis and Application of Transmission Line Conductors

Orin Laney
San Jose State University

ANALYSIS AND APPLICATION OF TRANSMISSION LINE CONDUCTORS

A Thesis

Presented to

The Faculty of the Department of Electrical Engineering

San José State University

In Partial Fulfillment

of the Requirements for the Degree

Master of Science

by

Orin Laney

August 2013

The Designated Thesis Committee Approves the Thesis Titled

ANALYSIS AND APPLICATION OF TRANSMISSION LINE CONDUCTORS

by

Orin Laney

APPROVED FOR THE DEPARTMENT OF ELECTRICAL ENGINEERING

SAN JOSÉ STATE UNIVERSITY

August 2013

Dr. Sotoudeh Hamedi-Hagh	Department of Electrical Engineering
Dr. Nader Mir	Department of Electrical Engineering
Dr. Robert Morelos-Zaragoza	Department of Electrical Engineering

ABSTRACT

ANALYSIS AND APPLICATION OF TRANSMISSION LINE CONDUCTORS

by Orin Laney

Skin effect is usually a concern reserved for radio frequency design and for high current conductors used in utility power distribution. Proximity effect between adjacent conductors has traditionally been a concern for the design of magnetic windings and other applications involving wire bundles. The rise in the ubiquity of high speed bit streams and other signals of very wide bandwidth has broadened the range of applicable contexts and increased the need to account for such effects. This is especially true for transmission lines used to interconnect critical signal paths in applications ranging from microelectronic devices to the signal integrity of printed circuit traces and implementation of system cabling.

Optimal conductor design is obviously fundamental to transmission line performance. Researchers have paid considerable attention to the topic but the results are scattered throughout the literature. This thesis collected information on extant conductor designs, and the theoretical considerations behind each solution. A detailed analysis of current flow in a conducting half-space was included as a foundation.

The conductor types discussed were solid cylindrical, rectangular, ribbonoid, bimetallic, tubular, laminated, litz, and stranded constructions. Discussions of the performance of stranded shields and conductor roughness effects were included for completeness of understanding.

DEDICATION

This work is dedicated to my late wife Lee, whose love of learning remains an inspiration, and to my new wife Toni, who continues the tradition and adds her own spice.

ACKNOWLEDGEMENTS

Thank you, Dr. Nader Mir, for patience, intelligence, and flexibility in leading the Analog / Mixed Signal program. I likewise thank Dr. Sotoudeh Hamedi-Hagh for intellectual inspiration and ready acceptance of the role of thesis advisor. Thank you, Dr. Robert Morelos-Zaragoza, for insightful comments and willingness to serve on short notice. Thank you, Dr. David Bruck, for your kind and professional assistance with administrative matters.

Appreciation is due Dr. Timothy Maloney of Intel and Dr. Darren Leigh of Tactual Labs for informal comments on the manuscript in progress. The patient support of staff at Mackichan Software in shepherding me through the wonders of the LaTeX language is also acknowledged. I thank my friend M. P. Schultz for able assistance with computer matters.

Above all, I thank the Hand of Divine Providence for all things that inspire, uplift, and edify.

TABLE OF CONTENTS

CHAPTER

LIST OF TABLES

Table

LIST OF FIGURES

Figure

CHAPTER 1

INTRODUCTION

An ideal transmission line has zero loss, a fixed real impedance, constant propagation delay per unit length, and infinite bandwidth. For a coaxial configuration, the outer conductor acts as a perfect separator between the outside world and internal propagation. Ideal transmission lines are made of pure unobtainium.

The performance of real cables is limited by available materials. The finite conductivity of metals adds a series loss term to the characteristic equations. Likewise, dielectrics have finite resistivities that add a shunt loss term. The more important consideration for real cables is that parameters change with frequency. The DC series loss term is readily swamped by skin effect contributions as frequency increases. Similarly, the DC shunt resistivity contribution is generally miniscule compared to AC dielectric losses [1].

The reactive components of cable characteristics are of equal importance. Skin effect reduces the contribution of internal inductance to total inductance. One result is a shift in characteristic impedance in the transition region between DC to low frequency operation and higher frequency characteristics [2].

Distributed capacitance is generally a reliable number only because stable materials are usually chosen. Inexpensive microstrip and stripline substrates are sometimes inconstant. For instance, lesser grades of FR-4 laminate are notorious for a shift to a lower dielectric constant in the UHF region [3][4].

Above and beyond the effects of materials choices, real transmission lines are

creatures of their construction. A common scheme classifies coaxial cables according to the mechanical formability of their shields, describing them as flexible, semi-flexible, semi-rigid, or rigid types [5]. These differing constructions have implications for signal ingress/egress and ultimate attenuation. Center conductors likewise have construction choices that affect performance for better or for worse.

Thus it is that the simple equations describing ideal transmission lines, though invaluable for conceptual purposes, are often insufficient descriptors of realizable designs. The purpose of this thesis is to bridge between the world described by ideal equations, and the realities of physical, non-ideal transmission lines. It augments the classic theory taught to undergraduates, and illuminates subtleties that can be variously detrimental or advantageous according to their treatment.

Here, the term "transmission line" specifically refers to TEM mode[1] lines (quasi-TEM for microstrip). The emphasis is coaxial construction, but mostly in the context that a coaxial current return path offers minimum complexity of analysis rather than the properties of coaxial transmission per se.

The thesis first addresses the mathematical description of skin and proximity effects before considering the implications of eight types of physical center conductor construction. This is followed by discussion of braided shields and the effects of surface roughness. Each of these topics has its own body of literature, which is reviewed as each topic is addressed.

Conclusions reached are generally applicable to any TEM transmission line. Microstrip and stripline constructions are covered where discussed effects are deemed significant to their application. Relevant microelectronic considerations are included.

---

[1] Transverse electromagnetic (TEM) modes are characterized by no electric or magnetic field in the direction of propagation.

CHAPTER 2

SKIN EFFECT AND PROXIMITY EFFECT

2.1 Skin Effect

Around 1880, a worker isolated with respect to ground held a large iron bar in his hands with the intent of short circuiting the terminals of a high capacity dynamo used in electroplating. The instant contact was made, he dropped the bar and claimed it burned his hands. The bar was carefully picked up, but was nearly cold. What happened? Skin effect forced the rapidly changing current to flow in a thin surface layer that instantly heated enough to burn skin. Within seconds of being dropped, the surface heat diffused into the bulk, leaving the bar only lukewarm [6].

Skin effect and proximity effect are consequences of the minus sign in Faraday's law of induction. Simply put, a changing magnetic field induces circulating ("eddy") currents in conductors immersed in that field, including in current carrying conductors that are the source of the field. Eddy current circulation is always in the direction that creates a magnetic field opposing the change in the original one. Many consequences arise from this phenomenon, from eddy-current-driven heat loss in the core of a laminated transformer to the ability of a superconductor to levitate a permanent magnet.

Skin effect is a well explicated phenomenon. The classic 1942 paper by Wheeler discussed the effect in detail [7]. Even today, researchers explore ways to describe the effect from novel viewpoints, specific approaches to modeling, and new solution methods [8], or for particular physical situations.

Understanding skin effect in current carrying conductors and proximity effect

in nearby conductors is fundamental for the design of well-behaved electrical transmission lines. These effects increase the losses of such lines but, more importantly, the losses vary with frequency. It is the latter fact that prevents trivial compensation for their presence. These losses must be managed to attain maximum transmission line performance.

2.2 Analysis of a Conductive Half-space

A logical starting point for examination of skin effect is the case of a conductive half-space (a plane conductor of infinite depth). This configuration avoids geometric complications and allows further extension of results to cases where the physical situation represents a valid approximation to the infinite depth case.

2.2.1 Mathematical Description of Current Flow

Let the yz plane define the surface of a half space of infinite depth for $x \geq 0$. Let surface current density be uniform and cosinusoidally excited. Classical EM theory predicts that current density in the slab will decay exponentially with depth with an associated phase retardation of 1 radian per neper [7]. The amplitude and phase describe a decaying spiral in the complex plane.

Let the 1 neper distance ("skin depth") $= \delta$, and let peak surface current density $J_z(x = 0) = J_0$ *Amp/meter*. Then current density at any point inside the half space is:

$J_z(x) = J_0 e^{\frac{-x}{\delta}} \cos(\omega t - \frac{x}{\delta})$ (starting assumption)

$= J_0 e^{\frac{-x}{\delta}} \left(\cos(\omega t) \cos\left(\frac{x}{\delta}\right) + \sin(\omega t) \sin\left(\frac{x}{\delta}\right)\right)$ (trig identity)

Summing current density in the x direction yields current referenced to the surface:

$$I_z(x) = \int_0^\infty J_z(x)dx$$

$$= J_0 \cos(\omega t) \int_0^\infty e^{\frac{-x}{\delta}} \cos\left(\frac{x}{\delta}\right) dx + J_0 \sin(\omega t) \int_0^\infty e^{\frac{-x}{\delta}} \sin\left(\frac{x}{\delta}\right) dx$$

$$= J_0 \frac{\delta}{2} e^{\frac{-x}{\delta}} \left[\cos(\omega t)\left(\sin\frac{x}{\delta} - \cos\frac{x}{\delta}\right) - \sin(\omega t)\left(\sin\frac{x}{\delta} + \cos\frac{x}{\delta}\right)\right]\Bigg|_0^\infty \qquad (2.1)$$

$$= J_0 \frac{\delta}{2} (\cos\omega t + \sin\omega t)\, amps/meter \text{ (summary result)} \qquad (2.2)$$

The time domain terms tell us that the spiral rotates ω radians per second, but this is ignorable for present purposes. Here, the importance of ω is that it determines skin depth.

The proportionality between current magnitude and skin depth is a consequence of constraining surface current density to a fixed value. From this viewpoint, increased skin depth equals greater current flow *for the same surface current density.* In the alternative, if current was the fixed quantity, then increased skin depth would result in decreased current density at the surface. The two viewpoints are conceptually equivalent.

After manipulation, equation 2.1 can be restated as:

$$I_z(x) = -J_0 \frac{\delta}{2} e^{\frac{-x}{\delta}} \left(\cos(\omega t - \frac{x}{\delta}) + \sin(\omega t - \frac{x}{\delta})\right) amps/meter \text{ for } x \geq 0. \qquad (2.3)$$

The leading minus sign is a consequence of the direction of integration. It is cancelled when the results at $x = \infty$ and $x = 0$ are subtracted to evaluate the integral. The minus sign is easily avoided by reversing the direction of integration when convenient, i.e.

$$I_z(x) = \int_{\infty}^{0} J_z(x)dx = J_0 \frac{\delta}{2} e^{\frac{-x}{\delta}} \left(\cos(\omega t - \frac{x}{\delta}) + \sin(\omega t - \frac{x}{\delta})\right)\Big|_{\infty}^{0} \; amps/meter \quad (2.4)$$

Although the answer simplifies to the summary result, inspection of the equation before evaluation yields a more nuanced picture of current flow. Taking the surface current density as phase reference, the cosine term represents real current flow and the sine term represents reactive current. Real current flow is forward wherever $\cos(\frac{x}{\delta}) > 0$ and reversed where $\cos(\frac{x}{\delta}) < 0$. Similarly, reactive current is inductive where $\sin(\frac{x}{\delta}) > 0$, and capacitive where $\sin(\frac{x}{\delta}) < 0$.

Real and reactive currents overlap, but the relationship between phase and depth means the forward and reverse currents are spatially separated. Likewise, the inductive and capacitive currents are separate with respect to each other. Each current component is the sum of an infinite number of regions of similar flow but decaying amplitude in the depth of the half space. Normalized to a surface current density of 1A/m, detailed analysis (appendix A) shows that the magnitudes of the individual current components are:

Table 2.1: Current Components

Flow	**Magnitude**
Forward	608.6 mA
Reverse	108.6 mA
Inductive	522.6 mA
Capacitive	22.6 mA

The decay of amplitude with depth means that the sum of forward current flows dominates that of the deeper reverse flows. Therefore, net real current is

necessarily forward. Similarly, the inductive fraction of reactive current dominates the capacitive contribution so that the net is always inductive. A good conductor applied below optical frequencies can have only a vanishingly small displacement current, therefore the "capacitive" current is solely an artifact of propagation delay of the evanescent wave into the conductor interior. By the same reasoning, so are the inductive and reverse real currents.

2.2.2 Power Loss Calculation

Spatial separation of opposing current flows means they do not cancel with respect to power loss. Power loss for forward and inductive flows is the price for sending current through the conductor. Reverse and capacitive flows are parasitic terms that dissipate power without any commensurate benefit.

Let ρ equal material resistivity. Power loss density at any point in the bulk conductor is:

$$\rho J_z^2 = \rho \left(J_0 e^{\frac{-x}{\delta}} \cos(\omega t - \tfrac{x}{\delta}) \right)^2 = \rho J_0^2 e^{\frac{-2x}{\delta}} \tfrac{1}{2}(1 + \cos(2\omega t - \tfrac{2x}{\delta}))$$
$$= \rho J_0^2 e^{\frac{-2x}{\delta}} \tfrac{1}{2}(1 + \sin(2\omega t)\cos(\tfrac{2x}{\delta}) - \cos(2\omega t)\sin(\tfrac{2x}{\delta}))\ watts/m^3$$

Let I_z equal the z-directed current flow referenced to the surface of the yz plane. Power referred to the surface is: $P = \rho I_z^2$. I_z^2 is found in turn by integrating $J_0^2 e^{\frac{-2x}{\delta}}$ throughout the depth of the half-space. Let $\frac{x}{\delta} = \xi$. Then:

$$P = \rho J_0^2 \frac{1}{2} \left(\int_\infty^0 e^{-2\xi} d\xi + \sin(2\omega t) \int_\infty^0 e^{-2\xi} \cos(2\xi) d\xi - \cos(2\omega t) \int_\infty^0 e^{-2\xi} \sin(2\xi) d\xi \right)$$

$$= \rho J_0^2 \frac{1}{2} \left(\frac{1}{2} + \frac{1}{4} \sin(2\omega t) - \frac{1}{4} \cos(2\omega t) \right) \tag{2.5}$$

$$= \frac{\rho}{8} J_0^2 \left(2 + \sin 2\omega t - \cos 2\omega t\right) watts/m^2 \tag{2.6}$$

Minimum power is $\frac{\rho}{8}J_0^2\left(2-\sqrt{2}\right)$, maximum power is $\frac{\rho}{8}J_0^2\left(2+\sqrt{2}\right)$, and average power is$\frac{\rho}{4}J_0^2$. Although $I_z(t)$ passes through zero twice per cycle, at no instant of time does $P(t)=0$.

2.2.3 Applicable Metrics

The decay of current amplitude with depth follows the same mathematics as decay with respect to time. Therefore, metrics applicable to either context can be used in the other. Starting from the definition of δ, an amplitude decrement of 1 neper over a phase change of 1 radian imputes a quality factor $Q=\frac{1}{\sqrt{2}}$.

$$\delta(f,\rho,\mu)=\sqrt{\frac{\rho}{\mu\pi f}}\approx 0.5642\sqrt{\frac{\rho}{\mu f}} \tag{2.7}$$

$$\delta(f,\rho,\mu_r)=\sqrt{\frac{\rho}{\mu_0\mu_r\pi f}}=\sqrt{\frac{10^7}{4\pi}\frac{\rho}{\mu_r\pi f}}\approx 503.3\sqrt{\frac{\rho}{f\mu_r}}meters \tag{2.8}$$

$$\delta_{Cu}(f)=\sqrt{\frac{10^7}{4\pi^2}\frac{1.678*10^{-8}}{f}}\approx 0.0652f^{-\frac{1}{2}}meters=65.2f^{-\frac{1}{2}}mm \tag{2.9}$$

Interior conduction can be modeled using cascaded L/R time constants [9], for instance as illustrated in figure 2.1.

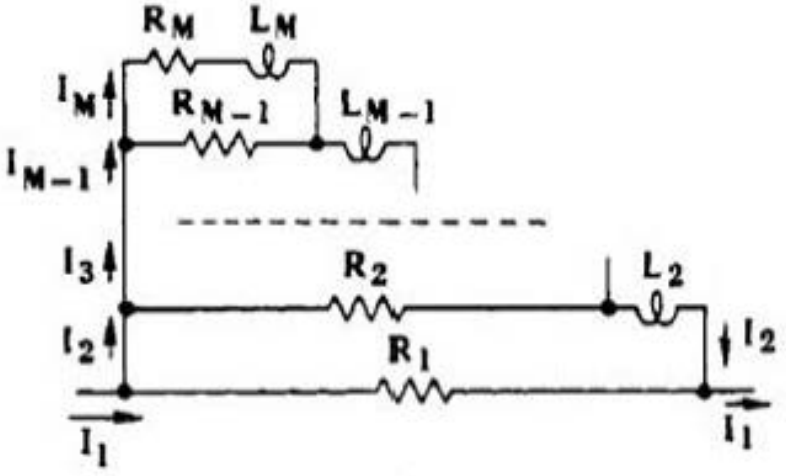

Figure 2.1: Example of a cascaded L/R model (Yen)

The distributed L/R time constants that characterize the conductor act as a low pass filter for signals propagating normal to the surface. The 3 dB corner frequency is a function of depth. Given that -3 dB equates to a $\frac{1}{\sqrt{2}}$reduction in amplitude, solving $\delta = \sqrt{\frac{\rho}{\pi f \mu}}$ for f_{3dB} yields

$$x_{3dB} = \delta \ln \sqrt{2} \approx 0.3466\delta \tag{2.10}$$

$$f_{3dB}(x, \rho, \mu) = \frac{\ln^2 2}{4\pi} \frac{\rho}{\mu x^2} \approx 3.8233 * 10^{-2} \frac{\rho}{\mu x^2} \frac{Hz}{m^2} \tag{2.11}$$

$$f_{3dB}(x, \rho, \mu_r) = \frac{\ln^2 2}{4\pi} \frac{10^7}{4\pi} \frac{\rho}{\mu_r x^2} \approx 3.0425 * 10^4 \frac{\rho}{\mu_r x^2} \frac{\mathrm{Hz}}{\mathrm{m}^2} \tag{2.12}$$

$$f_{3dB}(x, Cu) = \frac{10^7}{4\pi} \frac{\ln^2 2}{4\pi} \frac{1.678 * 10^{-8}}{x^2} \approx \frac{5.1053 * 10^{-4}}{x^2} \frac{Hz}{m^2} = \frac{510.53}{x^2} \frac{Hz}{mm^2} \tag{2.13}$$

For example, at a depth of $100\mu m$ in copper, $f_{3dB} \approx 51.05kHz$. As another example, given δ for 60 Hz in any good conductor, $f_{3dB} \approx 7.2$ Hz at the same depth.

Radial velocity into the interior of a good conductor is orders of magnitude slower than longitudinal propagation at the conductor surface. The relationship of 1 radian per skin depth δ equates to a velocity

$$f\lambda = \omega\delta = \omega\sqrt{\frac{\rho}{\pi f\mu}} = \sqrt{\frac{4\pi^2 f^2 \rho}{\pi f\mu}} = \sqrt{\frac{4\pi f\rho}{\mu}} m/s \tag{2.14}$$

$$velocity(f,\rho,\mu) = \sqrt{\frac{4\pi f\rho}{\mu}} \approx 3.5449\sqrt{\frac{f\rho}{\mu}} \tag{2.15}$$

$$velocity(f,\rho,\mu_r) = \sqrt{\frac{10^7}{4\pi}\frac{4\pi f\rho}{\mu_r}} \approx 3162.3\sqrt{\frac{f\rho}{\mu_r}} \tag{2.16}$$

$$velocity(f,Cu) = \sqrt{0.1678f} \approx 0.40963\sqrt{f} \tag{2.17}$$

The radial velocity in copper at 60 Hz is ≈ 3.2 meters per second. The $\sqrt{f}$ dependence of radial velocity means that the interior frequency response is dispersive. Although the highest signal frequencies arrive the fastest they are also the most highly attenuated. One consequence is that the velocity of a step function propagating into the interior, for instance measured as rise time to the 50% level, slows with increasing depth [10].

2.3 Case of Finite Depth

The preceding analysis suggests that a planar conductor thickness not exceeding the depth of the boundary between forward and reverse real flows would avoid the associated reverse flow loss term. This proves to be the case, resulting in lower loss than for an infinitely deep conductor.

Dwight [11] and others have determined that the normalized resistance of a flat, finite thickness plane conductor is:

$$\frac{R}{R_S} = \frac{\sinh(\frac{2x}{\delta}) + \sin(\frac{2x}{\delta})}{\cosh(\frac{2x}{\delta}) - \cos(\frac{2x}{\delta})} \tag{2.18}$$

,

which is plotted below in figure 2.2.

Minimum normalized resistance ≈ 0.91715, which occurs at $\frac{x}{\delta} = \frac{\pi}{2} \approx 1.5708$

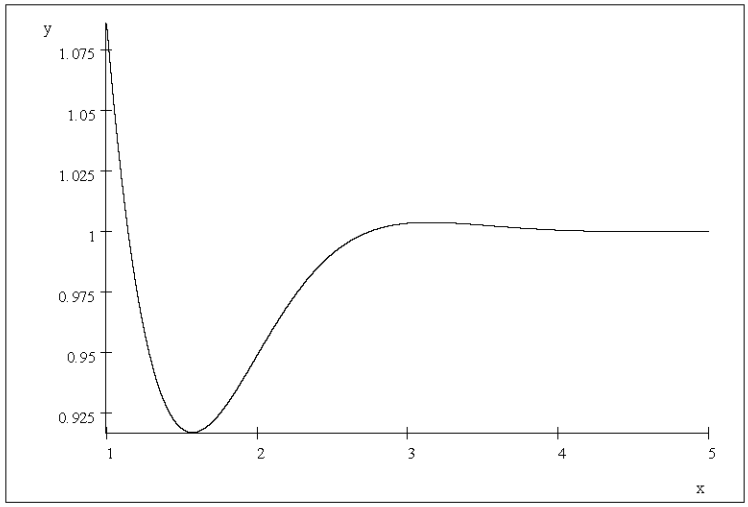

Figure 2.2: Normalized Resistance versus x/δ

There is an optimal thickness for any operating frequency and choice of conductor material. This is an important consideration for the design of, for instance, flat and tubular conductors.

2.3.1 Wideband Applications

Many applications involve bandwidths that extend considerably above and below the conductor optimum. Above f_{opt} for the conductor, performance

increasingly approximates the infinite depth case. At lower frequencies current density becomes increasingly uniform and resistance is asymptotic to the DC value, which is not zero as it would be for the case of infinite depth.

Below the transition region between low frequencies and the onset of skin effect, the flattened resistance versus frequency curve reduces phase and amplitude distortion, which improves signal fidelity. The ability to trade minimum loss for bandwidth flatness is a classic gain (loss)-bandwidth trade-off that can be used to optimize edge shape and pulse fidelity.

2.3.2 Cavities and Waveguides

The benefits of optimizing conductor thickness can be applied to resonant cavities and internal waveguide coatings (e.g. with gold or silver plating). For thin conductive coatings it should be noted that current flow on the far side of the conductive layer means that it is not of itself an effective shield. Backing with a material having low conductivity compared to the coating and adequate attenuation with depth is necessary to provide high levels of shielding.

Magnetic alloys such as mild steels have $\approx 20X$ the resistivity of copper and minimum $\mu_r \approx 300$ at low induction, with resulting attenuation at least 15 dB greater than copper of the same thickness at much lower cost. Transformer grade steel (3% Si) offers resistivity $\approx 28X$ that of copper and initial permeability $\approx 2000\mu_r$, for attenuation at least 28 dB greater than the same thickness of copper. The outer walls of RF anechoic chambers are commonly fabricated from sheet steel.

For applications requiring exceptional dimensional stability, invar alloy offers a resistivity $\approx 50X$ that of copper and minimum $\mu_r \approx 1000$ [12]. The resulting skin depth is $\approx 22\%$ that of copper. Invar offers attenuation ≈ 30 dB greater than the same copper thickness.

2.4 Proximity Effect

Just as skin effect causes AC currents to concentrate near the surface of a conductor, conductor to conductor coupling causes an equivalent proximity effect between conductors. Skin effect itself can be described as a "self-proximity effect" in which the interacting conductors are coincident. There are two cases of proximity effect, depending on whether the proximal currents are parallel or anti-parallel.

For parallel currents, proximity effect concentrates current density in regions of farthest proximity, exactly as skin effect does inside individual conductors. This applies, for example, to stranded conductors. Anti-parallel currents concentrate in regions of closest proximity, for instance in TEM transmission lines, which by definition have anti-parallel forward and return current paths. In either case, proximity effect raises apparent resistivity by channeling current through an effectively smaller cross section, above and beyond skin effect alone.

Interestingly, although parallel currents concentrate at points of farthest proximity, the physical force between conductors is attractive. Although antiparallel currents concentrate at points of closest proximity, the mutual force is repulsive. Thus, coaxial cable and other TEM transmission lines experience an expansive force between the forward and return current paths, as illustrated in figure 2.3.

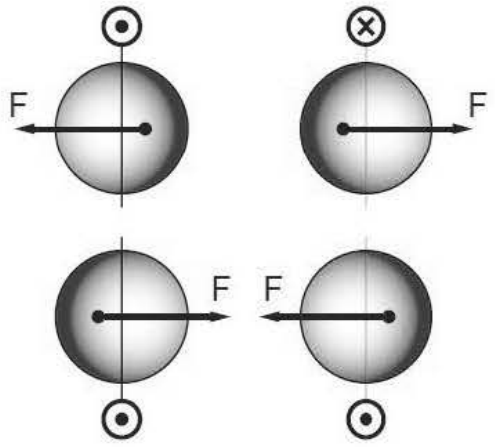

Figure 2.3: Current crowding and force direction

The case of a simple solenoidal winding is instructive. Each traveling electron is influenced by parallel current in adjacent turns, and by the same current viewed across the diameter as antiparallel. Thus, the forces on a solenoid are axially compressive and radially expansive. By virtue of charges traveling in parallel through it, an isolated conductor experiences both skin effect (at high frequencies) and a radially compressive force (always). The radial force (z-pinch effect) is what confines lightning discharges into narrow, discrete channels[1] [13][14].

Arnold derived formulas for proximity effect in hollow conductors [15]. Solid conductors are included by setting the inner radius to zero. Smith analyzed proximity effect for an arbitrary number of paralleled conductors [16].

[1] Typical channel diameters are in the range of 20 to 50 mm (Rakov). Odarn cites a nominal lower diameter limit and a nominal upper peak current limit when he observes, "An isolated conductor carrying a current suffers a radially inward pinching effect. Where the current is of sufficient magnitude to produce a very high surface magnetic intensity (of the order of several MA/m) severe mechanical distortion may occur. For example, a conductor of 5 mm diameter carrying a peak current of 200kA would experience a pressure of 1000 atmospheres (10^8 N/m^2)." For comparison, pressure at the bottom of the Marianas Trench is $\approx$ 1086 atmospheres (bars).

CHAPTER 3

CONDUCTOR CONSTRUCTION

Most analyses of coaxial transmission lines assume that the center conductor is solid and cylindrical. This is, however, one of eight alternatives. In their order of discussion, solid cylindrical conductors are foundational. Bimetallic conductors are derivative from cylindrical ones, and tubular conductors are a limiting case of bimetallic that segue into laminated construction. Rectangular forms are considered next and have frequency responses distinct from circular constructions. Ribbonoid conductors follow as a distinct limiting case. Lastly, divided conductors are discussed. Litzendraht construction is the insulated case, while stranded construction lacks formal insulation but may exhibit similar behavior.

3.1 Solid Cylindrical Conductors

Solid circular conductors are ubiquitous and geometrically simple. In the DC to low frequency region (DC-LF), current density is substantially uniform throughout the cross section. Impedance is dominated by DC resistance (DCR). The region between the DC-LF and HF cases has current density that is concentrated at the surface although the interior carries a meaningful fraction of total current. In the high frequency (HF) region, skin effect is well developed and current flow is restricted essentially to a small depth starting at the conductor surface, which allows simplified analysis as a circular approximation of a planar conductor.

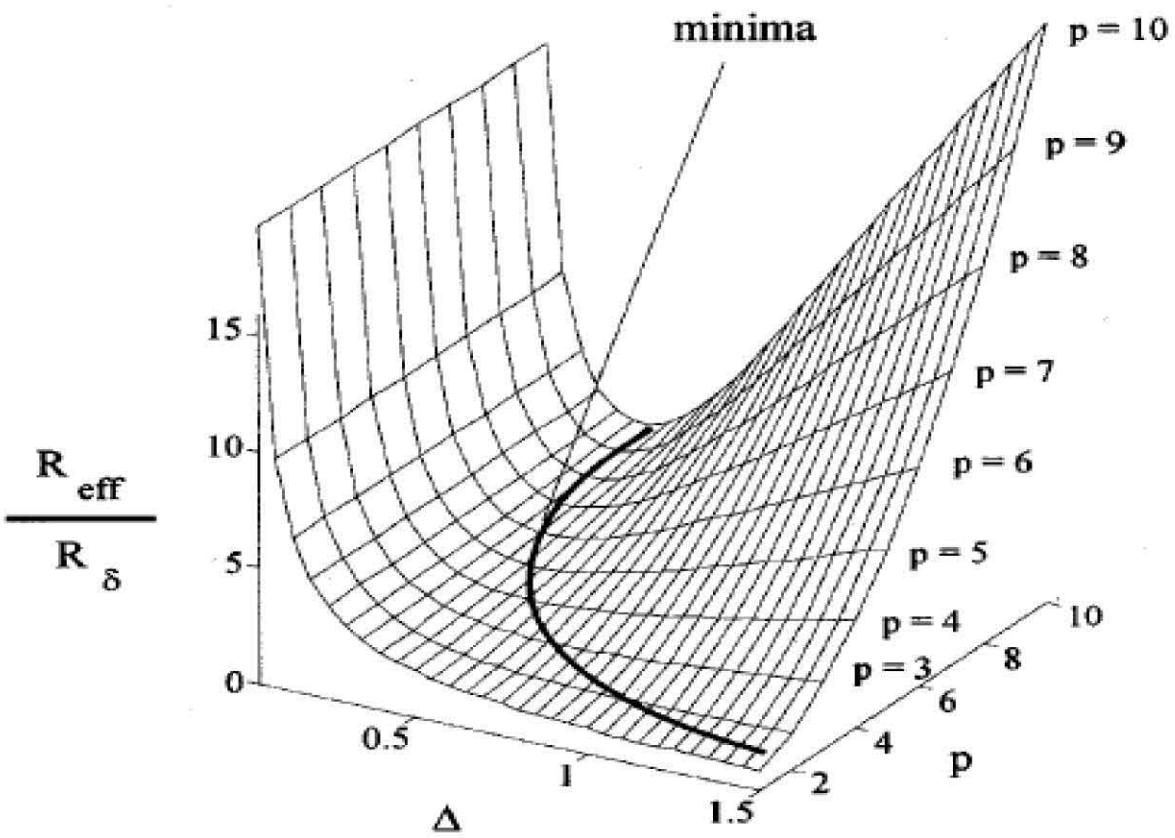

Figure 3.1: Normalized resistance vs δ normalized wire diameter and layer count

Unlike a plane of finite thickness, a cylindrical conductor in isolation has no optimum frequency. It is instructive to expand the context. Figure 3.1 shows the effect of adding winding layers to a transformer [17]. A single layer has a monotonic response, but two or more layers show an optimum frequency that becomes more pronounced and shifts as layer count is increased.

3.1.1 Copper Conductors

Two discrepant sets of physical constants are available for electrical copper. Many works continue to reference the International Annealed Copper Standard (IACS) established by the International Electrotechnical Commission in 1913. A complete set of wire tables based on this standard were published in 1914 in the Bureau of Standards Circular 31 [18]. The IACS standard specifies a copper resistivity of $1.7241 * 10^{-8}\ \Omega \cdot m$ and density of 8,890 kg/m^3 (20° C). It is customary to refer to conductor conductivity in terms of % IACS, with the standard value equaling 100%. For example, iron wire is $\approx$ 18% IACS [19].

Commercial copper processing has improved considerably since 1913, with a consequent rise in copper purity. One result is that the conductivity of ordinary commercial copper typically ranges between 101% to 103% IACS[1] . The resistivity of annealed, high purity copper electrical wire is $\approx 1.678 * 10^{-8}\ \Omega \cdot m$ (102.75% IACS, 20° C) [20].

Modern copper density likewise differs from the IACS value and is in the general range of 8920 to 8960 kg/m^3. The variance arises because density is determined by thermomechanical history as well as purity. The density of soft-drawn, annealed copper wire is $\approx$ 8924 kg/m^3 (20° C) [21]. The modern values are used herein, since they most closely match purchasable annealed wire.

[1] The conductivity of pure copper (99.999% Cu) is 103.06% IACS.

3.1.2 Gauge Systems

The American Wire Gauge (AWG) system was introduced by Brown & Sharpe in 1857. It is a simple but elegant system based on a geometric progression, and is specific to round copper wire and other nonferrous electrical conductors. Steels and other alloys have different drawing characteristics and use other gauge systems.

The starting stock for copper electrical wire is a cast rod that is pulled through a series of drawing dies. Per conservation of volume, this progressively reduces diameter while increasing length. Gauge is proportional to the number of draws required to reduce diameter to the wanted result. Consequently, finer wires have correspondingly higher gauge numbers.

Wire metallurgy and drawing technology have advanced over the years, and contemporary manufacturing may alter the number of draws to achieve a given diameter. This is transparent to the end user, for whom AWG tables remain an accurate guide.

Because copper becomes work hardened by wire drawing, intermediate wire is periodically annealed during the drawing process to restore ductility. Note that a manufacturer may omit final annealing of the completed wire as a means of slightly lowering cost. This product is stiffer than the annealed variety, which increases the difficulty of creating tight bends and conformal windings, particularly for larger diameter conductors. The conductivity is also lower, somewhat increasing electrical losses. It is the purchaser's responsibility to select or specify final annealing when these differences are important.

For reasons of economy and adequacy, many types of electrical wire are stocked only in even gauges. However, designers of transformers, inductors, motor windings, and the like specify magnet wire in single gauge, half gauge, or even third

gauge steps to optimize the performance of devices constrained by a limited winding cross section.

Standard Wire Gauge (SWG, formerly British Standard) is a system similar to AWG but empirical and irregular. Table lookup is required to convert between SWG and diameter. ISO gauge is conductor diameter specified in tenths of a millimeter, which imposes an inverted sense compared to AWG and SWG. Many metric wire tables sidestep the artifice by simply using millimeters [22]. The AWG system is used herein for mathematical simplicity, because AWG parameters are readily translatable to SI units, and because electrotechnical professionals are widely familiar with it.

3.1.3 Useful Formulas

The gauges of the AWG system can be calculated by noting that 4/0 gauge[2] has a 0.460000 inch diameter, while AWG 36 has a diameter of 0.005000 inch. Given the diameter ratio = 92 and the gauge range = 39 steps, a step ratio $\approx$1.1229322 is readily calculated. Noting that the sixth power of this ratio $\approx$ 2.005, a common rule of thumb is that a change of three gauge steps halves or doubles cross sectional area, and six steps halves or doubles diameter. The ratio to the 20th power is $\approx$ 10.15, therefore a change of 10 gauge steps will increase or decrease cross sectional area by approximately a factor of ten, while 20 gauge steps does the same for diameter [3] .

Diameter D_n for any given AWG = n can be found using:

[2] 4/0 (pronounced 'four aught') is equivalent to an AWG of negative three. This is a change of notation for gauges less than one. Zero gauge is 1/0, etc. This system ends at 7/0, beyond which diameters or cross sectional areas are used.

[3] These results are reminiscent of decibel calculations.

$$D_n \approx e^{-1.12436-0.11594n} inch \approx e^{2.1104-0.11594n} mm \tag{3.1}$$

Conversely, AWG can be calculated from diameter using:

$$AWG \approx -8.6249 \ln(d_{inch}) - 9.6975 \approx -8.6249 \ln(d_{mm}) + 18.2019 \tag{3.2}$$

The frequency at which skin depth δ = wire radius is the demarcation point between DC-LF conduction and skin-depth-limited conduction. Calculating the associated frequency is straightforward. The formula for skin depth is:

$\delta = \sqrt{\frac{2\rho}{\omega\mu}} = \sqrt{\frac{\rho}{\pi f \mu}}$ meters

Setting wire radius $r = \delta$ and manipulating terms, we obtain

$$f_{transition}(\rho, \mu, r) = \frac{\rho}{\pi r^2 \mu} Hz \tag{3.3}$$

Noting that πr^2 = cross sectional area a, and resistance $R = \rho\frac{l}{a} \longleftrightarrow \rho = a\frac{R}{l}$, given $\frac{R}{l}$ in ohms per meter:

$$f_{transition}(R, l, \mu) = \frac{1}{\mu}\frac{\Omega}{m} \tag{3.4}$$

$$f_{transition}(R, l, \mu_r) = \frac{10^7}{4\pi}\frac{1}{\mu_r}\frac{R}{l} \approx 7.9577 * 10^5 \frac{1}{\mu_r}\frac{\Omega}{m} \tag{3.5}$$

If $\frac{R}{l}$ is in ohms per kilometer:

$$f_{transition}\left(R, l, \mu_r\right) \approx \frac{800}{\mu_r} \frac{\Omega}{km} \tag{3.6}$$

for any good conductor material.

Substituting AWG = n for radius yields:

$$f_{transition}\left(\rho, \mu, n\right) \approx \frac{\rho}{\mu} e^{0.23189n+9.8363} \tag{3.7}$$

For copper, $\frac{\rho}{\mu} \simeq 1.335 * 10^{-2}\ \frac{\Omega}{A}$. Therefore,

$$f_{transition}\left(Cu, n\right) \approx e^{0.23189n+5.5203} \approx 250e^{0.232n} \tag{3.8}$$

Appendix B contains a table of $f_{transition}$ and other selected parameters for round copper wire.

3.2 Bimetallic Conductors

Bimetallic conductors commonly place a lower resistivity outer material over a high resistivity inner material. The use of two metals offers some of the advantages of each, such as high frequency conductivity plus mechanical strength, or reduction of noble metal content.

3.2.1 Copper Clad Conductors

Copper-clad steel (CCS), also known as copper-covered steel and by the trade name Copperweld[4] is a commercially important bimetallic conductor. Another is copper-clad aluminum (CCA) [23].

[4] Trademark of Fushi Copperweld Inc.

CCS is often used for the center conductor of coaxial cables. It has lower cost compared to solid copper of equal cross section. At high frequencies skin effect restricts current essentially to the copper alone, resulting in no significant performance difference.

A use consideration for exposed, larger diameter conductors such as for safety grounding in power utility distribution systems is the reduction of scrap value to essentially that of steel alone, which deters theft driven by high copper prices [24]. The copper jacket also confers superior corrosion resistance.

The general industry standard for CCS conductors is ASTM B452 [25]. Commercial CCS offerings have DC conductivities ranging typically from 15% to 70% of copper wire of the same diameter. Thin copper cladding is created using plating technology. A typical manufacturing process for high copper content casts molten copper around a steel rod. The resulting cylindrical billet is passed through a wire drawing process to the wanted diameter. The finished CCS retains the original copper-to-steel diameter ratio.

3.2.2 Reliability Considerations

The steel content of CCS provides much lower failure rates than copper alone. Solder or crimp termination of any conductor to a connector pin results in concentration of mechanical stress at the joint. Copper is a relatively soft metal with a tensile yield point around 70 MPa. Tension or dynamic flexure near the connector can result in breakage failure, especially for smaller wire diameters.

Steels for MIL-DTH-17H compliant coaxial cable have minimum yield points $\approx$345 MPa and are considerably more resistant to metal fatigue [26]. CCS fabricated per ASTM B869 (center conductors for CATV drop wire rated cable) has 21% conductivity and a minimum tensile strength of 827 MPa [27]. CATV

connectors typically avoid soldered or crimped center pins by using the stiff CCS center conductor itself as the male mating element, eliminating breakage as a failure mode. For drop wire, another purpose of the steel content is support of cable runs suspended in air.

3.2.3 Other Outside Metals

Any copper surface may be silver plated to reduce high frequency attenuation. This is a de facto bimetallic construction at sufficiently high frequencies, but the conductivity of silver is only about 6% more than that of copper, and plating is typically quite thin (tens of microinches). Therefore, for most purposes the silver can be considered as one with the copper despite being distinct metals.

Gold plating is used where corrosive environments are at issue. Due to high cost, gold plating is generally limited to short distances and small surface areas, such as for component leads or connector pins [28][29]. It is sometimes used as a finish for printed circuit traces to improve shelf life. Excess gold in soldered connections can create brittle intermetallic compounds that reduce joint reliability [30]. Therefore, gold plating thickness is usually not more than a few tens of microinches.

Nickel can be applied to copper to improve resistance to corrosion. It is also used as a barrier metal gold and copper or tin and copper, for instance in printed circuit finishing processes. Although far less expensive than gold, it has magnetic properties that can create slight nonlinearities in response to changing currents [31]. This is an issue in sensitive communication systems where the nonlinearity can create detrimental intermodulation products [32].

Wire manufacturers also offer pre-tinned copper wire. Tinning improves solderability during assembly and serves as a chemical barrier where direct contact between bare copper and certain types of covering insulation would cause an adverse

chemical reaction [33]. Tinned copper is an inverted bimetallic construction, in that the tinning alloy[5] has lower conductivity (and a rougher surface) than the underlying copper. The use of tinned center conductors in transmission lines is generally restricted to shorter cables and/or lower frequency uses, where the electrical performance degradation is minimal.

Galvanized steel is sometimes used for safety grounding where the conductor is exposed to the environment. Such conductors are adequate for transient fault currents and lightning diversion but generally not for steady power conduction because of high losses. Electric fences often use this material on the basis of adequacy and low cost. Galvanized steel is also used for electrical conduit.

3.2.4 Experimental Results

The academic literature on bimetallic conductors is somewhat sparse. In 1915, J. M. Miller published a study of the electrical resistance of CCS conductors for frequencies up to 3 KHz using simplified assumptions [34]. Teare and Webb published a more thorough analysis in 1943 [35] that included the case of arbitrary resistivity and permeability in both conductor layers. They found that the steel content of CCS is relevant only for fairly low frequencies.

Steel resistivities vary with alloy but are generally between 10^{-7} and 10^{-6} $\Omega \cdot m$, or $\approx$ 6 - 60 times that of copper. A general value of 20X serves as a rule of thumb. For CCS conductors with appreciable copper content, the steel carries only a small fraction of total current clear down to DC.

For the particular specimens studied by Teare and Webb, the difference between CCS conductivity and that of a hollow copper tube was less than 4% at 10

[5] Tinning for electrical conductors is typically a tin and lead composition per specifications MIL-P-81728, MIS-41177, or ASTM B579. The inclusion of lead suppressess tin whisker formation.

kHz. At 20 kHz, the tube approximation was as good as the accurate calculation. The CCS conductor had lower resistance than a hollow copper tube up to 85 KHz. In the region between 85 kHz and 160 kHz (the highest frequency studied), the copper tube approximation had lower resistance. This is consistent with the literature on hollow, tubular conductors (section 3.5).

More recently, Fei et al analyzed CCS performance in terms of reflection of the radial wave at the copper to steel interface [36]. They determined that the resistivity minimum corresponds to normalized copper depth $\frac{x}{\delta} = \frac{\pi}{2}$ wavelengths at the optimum frequency. Figure 3.2 illustrates the differing performance for two bimetallic conductors of equal outer diameter but changed copper content.

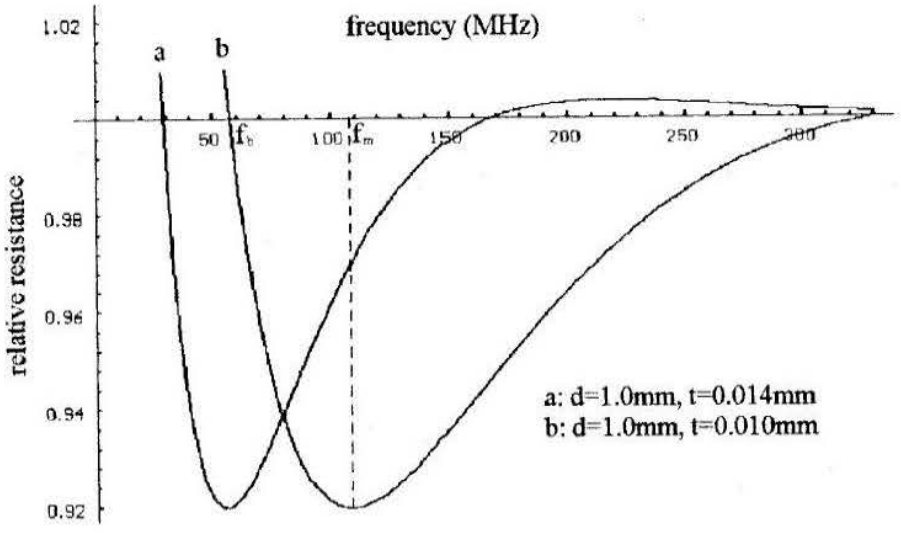

Figure 3.2: Minimum resistance curves for two CCS variants (Fei)

3.2.5 CCS Magnetic Circuit

Steel is used as the core for CCS because it is inexpensive and rugged, typically not for any magnetic properties. Miller noted that the magnetic field

associated with internal current travels through steel or copper alone only if each layer is perfectly round [34]. Figure 3.3 shows the cross section of an early specimen of CCS (contemporary processes are more tightly controlled). It is apparent that the crystal structure of the steel caused irregularities at the steel to copper interface. The effect of departure from circularity is to include some copper in the outermost portion of the magnetic circuit of the steel, which reduces the effective permeability of the steel in that region.

Miller suggested a slotted CCS conductor cross section as shown at the right of figure 3.3. Copper fills the slots. This interruption of the magnetic path in the steel more completely approximates a nonmagnetic core. The reduction in low frequency inductance means that the internal inductance of the wire changes less between the low frequency and high frequency regions, and therefore the curve of impedance versus frequency is flatter at the low end. This improves pulse fidelity.

Substitution of austenitic (non-magnetic) stainless steel or other alloys is another approach. Solder wettability of the core can be an issue if the copper layer is thin and therefore easily dissolved in solder.

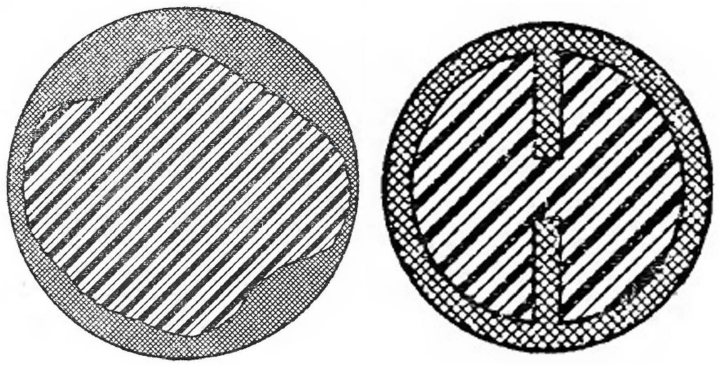

Figure 3.3: Example AWG8 cross section & Miller proposed

3.3 Tubular Conductors

A tubular conductor can be viewed as the limiting case of arbitrarily increasing the inner bulk resistivity of a bimetallic conductor. The conductor interior might be literally hollow (air filled) or metal covered dielectric [37]. The cross section is not necessarily circular.

Tubular construction is important for a number of compelling reasons. Obviously, it avoids the needless cost penalty of solid copper at high frequencies. Consistent with the discussion of bimetallic conductors, of equal or greater importance is that under the right conditions, hollow conductors offer lower loss than solid ones [38][39].

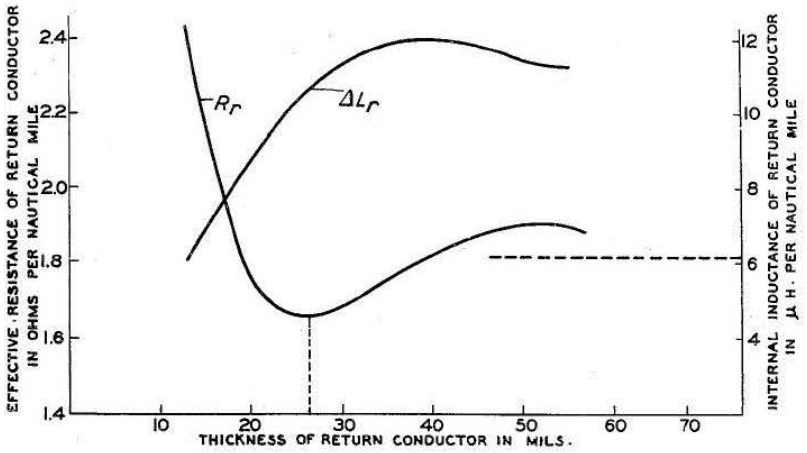

Figure 3.4: Example R and L vs tube thickness at fixed frequency. (Eglin)

Carson patented a concentric tubular transmission line (solid shield coaxial cable) in 1931 on behalf of AT&T [40]. The patent document contains a reasonably complete exposition on the mathematics of the system. Arnold published formulas for the AC resistance of isolated and concentric tubular conductors in 1936 [41], and Coufal also analyzed the case of concentric tubular conductors in 2007 [42], and

commented on skin effect in solitary tubular conductors.

For wideband signals best characterized in the time domain, for instance high speed serial bit streams, bimetallic and tubular conductors offer an important advantage in terms of pulse fidelity. The higher initial resistivity at low frequencies leads to a flatter frequency response in this region and therefore reduced phase distortion [43]. For many applications the increased low frequency attenuation is not an issue.

One example of tubular design is high power (tens to hundreds of kilowatts) coaxial transmission lines for broadcast use. These air dielectric lines use concentric copper tubes with outer diameters up to 9 inches or more [44]. The complete line is made by bolting flanged sections together. Individual section lengths are randomized by 10% or so to avoid additive effects from slight impedance discontinuities at the joints.

The tubular inner conductor is selected for current carrying capacity, while the outer conductor is sized for correct impedance. The large diameters arise from two considerations. One is the necessary spacing for the voltages involved. The other is provision of adequate surface area for the current magnitude in order to keep losses low [45].

The use of gas dielectric allows the line to be pressurized with dry air or nitrogen so that minor leaks do not allow entrance of water and other contaminants. A flow gauge in series with the pressure source provides a check of the mechanical integrity of the line.

On the electrical side, air or nitrogen has an $\epsilon_r \approx 1$, which keeps propagation velocity as high as possible, further lowering losses.

3.4 Laminated Conductors

Laminated conductors use nested tubular conductors with insulation between layers. The return conductor can be solid or also of laminated construction. Dwight studied current division in nested tubular conductors in 1942 [46]. By including dielectric effects, A. M. Clogston determined that skin effect losses could be greatly reduced, and articulated the laminated conductor concept in 1951 [47] as illustrated in figure 3.5. Among other experiments, the theory was verified with a coaxial resonant cavity having a 50 layer inner conductor [48]. Modern analytical tools such as computer based matrix techniques, have contributed to the recent study of laminated conductors [49]. Numerical optimization has established that efficient designs are possible using variable spacing and a more modest number of layers than otherwise [50].

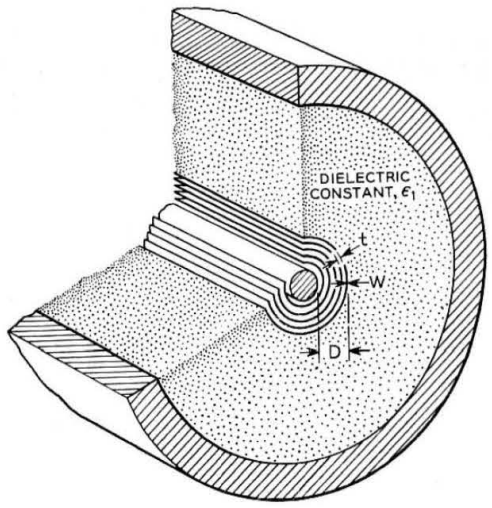

Figure 3.5: Cross section of Clogston design

The potential advantages of laminated construction are considerable. Laminated conductors offer a radical reduction in skin effect losses. Collective skin

depth can greatly exceed that of a solid conductor, with the result that the AC resistance of a laminated conductor can remain nearly equal to DC resistance over a considerable bandwidth. Thus, the advantage is not merely reduction of loss, but also flatness of response. Even a minimal design of two layers inside a coaxial return lowered attenuation by 20% from that of a solid inner conductor [51]. The lamination concept has also been studied in the context of shielding walls and resonant cavities [52].

It is not sufficient merely that layers are present and insulated from each other. Individual layers must be thin compared to the skin depth of a solid conductor, and therefore many layers are required to provide sufficient conductive cross section. A critical factor is that the internal and external velocities of propagation must be matched and uniform throughout the cross section. This requires proper attention to layer thickness and dielectric constants. Since internal propagation velocity is constrained by practical material choices, in general the external velocity must be slowed to match it. For this reason laminated conductors are generally studied in the context of coaxial construction, for which velocity can be manipulated through choice of dielectric constants.

The velocity of propagation in run-of-the-mill polyethylene dielectric coaxial cables is around 66% of free space. Experimental Clogston designs using polyethylene dielectric had velocities around 38%. Impedance was also lower than for commercial cables of the same outer diameter [53].

If the Clogston conductor can characterized as a parallel architecture, an interesting but apparently untested proposal is series lamination, in which the center conductor is implemented as a series stack of alternating metal and dielectric disks. The skin effect of the metal disks is countered by an opposing "bone effect" in the dielectric [54], which is the same principle used in the nested tube and

dielectric architecture of the Clogston design.

Laminated conductors remain an area for development. Clearly, it is infeasible to connectorize high layer counts. Connection to discrete parts such as resistors or semiconductor devices requires collapsing the layered structure into a solid termination. Such considerations plus difficulties of manufacture have kept laminated conductors largely experimental, with no catalog products found in a search of commercial suppliers of other conductor products.

3.5 Rectangular Conductors

Square and rectangular cross sections are often used to improve the packing density of stacked conductors. In larger sizes, they offer improved mechanical strength and ease of termination compared to round conductors. At high frequencies, they provide a higher ratio of surface area to cross section, reducing skin effect losses. Distribution of high current utility power is often based on rectangular busbars, making this a well studied case with results translatable to higher frequencies.

An often used assumption for determining the internal impedance of a conductor is the use of Wheeler's rule, which asserts that at high frequency the contributions from resistance and inductive reactance are of equal magnitude. This is easily shown to be the case for a conductive half-space, as recited in section 2.2.1, and also applies to the common case of cylindrical wire when skin effect is well developed.

Wheeler stated that his rule is valid only when the local radius of curvature is much greater than a skin depth. For a rectangular conductor, this caveat applies to corner curvature rather than overall dimensions. The result is greatly delayed

convergence to validity for Wheeler's rule as frequency is increased, even if corners are beveled or rounded.

Medina [55] critiqued the study of Antonini et al of the impedance of rectangular conductors [56], asserting that Wheeler's rule was adequate even for this case. In reply, Antonini et al noted that for a square conductor of half-width $= 350\delta$, the resistance to reactance ratio is 1.314:1. After increasing frequency by a factor of five to make half-width $= 782\delta$, the ratio is still 1.248:1 [57]. Clearly, the presence of 90 degree corners is problematic for Wheeler's rule despite skin effect being "well developed".

Other studies of rectangular cross sections corroborate this conclusion and reveal that, in general, resistive and inductive contributions of rectangular and ribbonoid conductors are not equal and must be determined numerically [58]. Shlepnev studied microstrip conductors and found convergence to Wheeler's rule at microwave frequencies ≈ 1 GHz [59]. Heinrich extended the Antonini results to the case of monolithic-microwave integrated-circuit coplanar waveguide [60].

Inductance formulas for rectangular and other conductors often use assumptions and approximations that can be problematic unless the assumed conditions are met [61]. Piatek and Baron [62] derived an exact formulation of the DC self-inductance of a straight rectangular conductor, but it is less numerically stable than formulations provided by Weeks et al [63], or Chen and Fang [64].

3.6 Ribbonoid Conductors

Ribbonoid conductors (also called strap or tape conductors and by other terms) are the limiting case of rectangular geometry. For purposes of analysis, theoretical thickness is often set to zero but the results apply to any rectangular

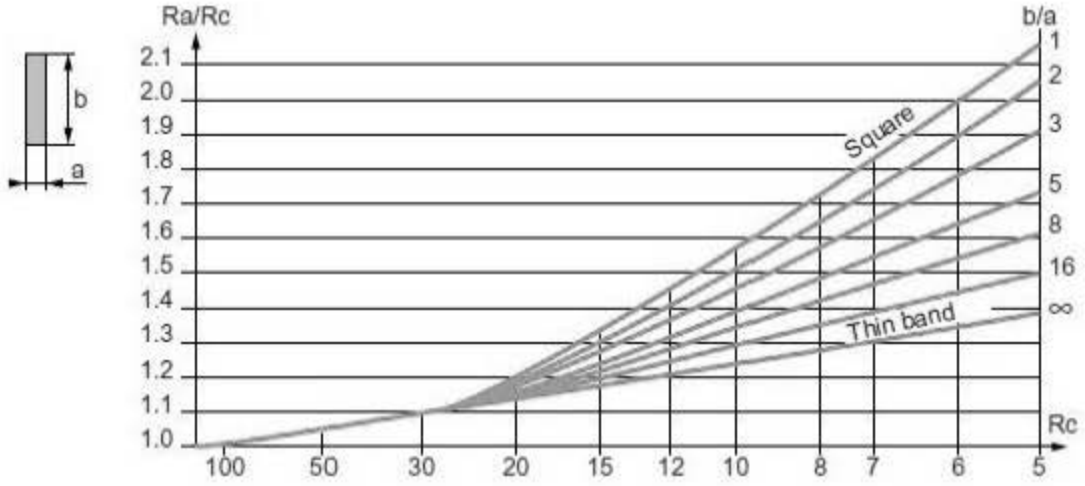

Figure 3.6: Extra skin loss vs frequency parameter for rectangular conductors

conductor with a width to thickness ratio $\gg 1$. Figure 3.6 shows the loss advantage of ribbonoid ("thin band") construction [65].

The foil conductors of printed circuitry are ribbonoid, as are thin film or evaporated metal conductors such as for metal-on-ceramic hybrid circuits or microelectronic devices [66]. In these applications thickness is usually fixed while width is determined by transmission line impedance for high frequency uses or by current carrying capacity for power transmission.

At low frequencies, both the width and thickness of a ribbonoid conductor are small compared to skin depth. In this instance, resistance per unit length is a simple matter of resistivity and cross sectional area, just as for any other conductor at a sufficiently low frequency.

For frequencies high enough to make skin depth smaller than the width dimension, a planar version of skin effect causes current crowding along the conductor edges. However, the entire cross section of the conductor remains available to carry the current distribution up to the limit where half thickness is

comparable to a skin depth. Because only the width dimension participates in skin depth limited conduction below the second limit, the difference between skin depth limiting in one dimension versus two dimensions creates a bandwidth advantage.

For ribbonoid ("thin tape") construction, Piatek and Baron [62] obtained a simplification of the general case formula for DC self-inductance:

$$L = \frac{\mu_0}{6\pi a^2}\left[3a^2 l \ln\frac{l+\sqrt{a^2+l^2}}{a} + 3al^2 \ln\frac{a+\sqrt{a^2+l^2}}{l} - \left(a^2+l^2\right)^{\frac{3}{2}} + l^3 + a^3\right] \quad (3.9)$$

This is the same as the formula derived by Hoer [67]. It has been noted that for certain geometries, this formula is not numerically well behaved. Ruehli [68] and Zhong [69] have each derived alternative exact solutions with improved numerical stability.

3.7 Litzendraht Conductors

The word "Litzendraht" is German for "braided wire". The essence of litzendraht ("litz") construction is conductive cross section built from multiple insulated wire strands. The purpose of braiding is to ensure that individual strands spend an equal fraction of the total length adjacent to the surface and to every other strand in the braid. Because all strands are alike in this respect, the result is equal current sharing among strands in defiance of skin effect. Note that it is not sufficient to simply twist multiple insulated strands together. Adequate transposition of the strands throughout the cross section is necessary to achieve the desired effect [70].

Individual strands must have diameters small enough to keep the current density in the cross section nearly uniform at the operating frequency. The result is

that the aggregate conducting cross sectional area is nearly equal to that of a single strand multiplied by the number of strands. Litz construction combines the current carrying capacity of a large (in terms of skin depth) conductor with the efficient use of cross sectional area offered by small conductors [71].

3.7.1 Cross Section Optimization

Determination of optimal strand diameter and number of strands is important for the case of litz based magnetic windings such as for power inductors and transformers [72]. Ferreira published methods for analytical computation of the AC resistance of round and rectangular litz construction [73]. The causes of loss and the effects of imperfect construction have also been studied [74].

The density of the working cross section is reduced by breaking it into multiple circular conductors, i.e. the areal coverage of a plane tiled with identical circles is $\approx$90.7%. Strand transposition reduces density compared to that achievable if strands maintained a fixed relationship. The need to insulate the strands further diminishes working density. Insulation coating processes for fine and ultrafine gauges typically add 5% to 10% to the diameter of the conductor. This sets a limit on the improvement possible for a fixed cross sectional area on the basis of diameter related loss reduction being offset by the insulation related decrease in total area [75].

End to end resistance is somewhat increased by the additional length required for the porpoised path each strand follows through the braid. This also mildly reduces the end to end velocity of propagation.

Attaining the litz advantage becomes increasingly difficult as operating frequency is increased. Specifically, diameter reduction to accommodate higher frequencies drives the strand count upward as the inverse square of strand diameter,

which rapidly increases cost. Achievable wire diameter has a practical lower limit. Venturing into hyperfine gauge territory is doubly problematic because cost per unit length zooms astronomically as this limit is approached. The simultaneous increase in required length and cost per unit length (see Appendix C) results in a formidable cost barrier.

The rapid increase in wire count associated with fine gauges has consequences for production handling. This is because each individual wire must be properly terminated if it is to participate in the total litz conductor. Ordinary commercial products subject to moderate temperature rises often rely upon "solderable" insulation [76] which melts at soldering temperatures, allowing soldering without insulation stripping. This allows dipping fluxed litz wire into a solder pot to simultaneously tin all wires into a solid termination. However, the finished state of individual strands at the center of the wire bundle cannot be ascertained, therefore it must be accepted that some small fraction might fail to connect properly

High reliability products generally require individually inspectable strand terminations. It is also common to require rugged, high temperature capable insulation that must be chemically or mechanically stripped. These requirements rapidly become infeasible for high wire counts.

Despite these considerations, litz wire can offer more efficient use of cross sectional area than a solid conductor dominated by skin effect, resulting in lower loss by comparison. However, the advantage of litz wire over solid wire of the same diameter is a sensitive function of operating frequency, strand diameter, and other parameters. Litz construction is most commonly applied to fixed frequency or narrowband situations where the loss advantage can be optimized by an application specific design.

It was noted that laminated conductors require many thin layers to provide

sufficient conductive cross section. In this sense, a laminated conductor is similar to litz wire, for which multiple small conductors provide aggregated conducting area. This suggests that litz conductors embedded in dielectric per Clogston doctrine may be an alternative route to the benefits of the Clogston design.

The costs and handling difficulties associated with fine and ultrafine wire limits the practical use of litz construction to frequencies typically not higher than the low MHz region. Some performance extension is possible through the obvious substitution of hollow or bimetallic conductors, but at higher frequencies low loss designs more typically rely upon simple conductors of sufficient surface area, such as bimetallic, tubular, rectangular, or ribbonoid constructions.

Consequently, although there are commercial offerings of coaxial cables with litz-based center conductors, such products are primarily application specific designs intended for high power audio, induction heating, and other high current uses involving modest frequencies. No litz-based coaxial cable products for general purpose use are found.

3.8 Stranded Conductors

Conductors built from multiple uninsulated strands are a staple of flexible conductor design. For a modest cost premium, they offer superior flexibility and bend life. The conductors distributing utility power in the walls of a home may be solid, but the cords of appliances plugged into receptacles will be stranded. Microphone cables are subject to severe dynamic flexure and internal conductors may parallel 100 or more fine gauge strands (e.g. AWG 44) to ensure adequate service life.

Strand counts generally adhere to numbers that optimally fill a circular cross

section. The first count that improves on a single conductor is seven, in which a central conductor is surrounded by six identical conductors in a second layer. For three layers, the optimal total is 19, for four layers it is 37, and for five, 61. In practice, counts higher than 19 may be arbitrary with conductors simply paralleled ("bunched") together for low cost. Structured designs achieve high counts by twisting stranded conductors into further optimal bundles, for example 7 bundles of 19 strands each for a total of 133.

Stranded conductors are not simply the subdivided equivalent of solid conductors. For example, the twist imparted to the strand bundle to keep it organized imparts an associated spirality effect that increases high frequency AC resistance [77]. It is also more difficult to quantify skin effect [78]. Consequently, the formulas used for solid conductors must be reinterpreted for stranded designs. There are various techniques to do this, such as a subdivision method for calculating frequency dependent resistance [79].

3.8.1 Strand Independence

It is widely supposed that uninsulated strands are well shorted to each other. Notwithstanding lack of insulation, adjacent strands may exhibit a surprising degree of independence [80]. Various considerations apply.

A geometric consideration is that parallel, touching cylinders contact each other along a one dimensional line of theoretically zero surface area. In practice, metallic conductors flatten somewhat along the line of contact, but resistive or insulative surface films, and bumps, ridges, and other asperities keep adjacent surfaces from fully intimate contact in the narrow shared width.

Some multilayered strand constructions alternate the handedness of twist for successive layers or use differing lay lengths on each layer. In this instance, layer to

layer strand contact occurs at discrete points rather than continuously along their lengths, further reducing the area of mutual contact. Appendix D discusses commonly available industry stranding styles.

Soldered contacts rely upon an alloyed bond. Pressure contacts such as between a wire and a screw head are able to achieve intimate, air excluded contact area through scouring and friction welding. However, parallel wires touching each other lack these mechanisms. There is a possibility that dust or other insulating contaminants might be present as a barrier. Thin oxide films might be present. These are easily broken by mechanical pressure, but even broken films may leave nanoparticles of oxide residue between lightly touching metal surfaces. Given the conductivity ratios between oxides and their respective metals, this may suffice to channel current primarily through individual conductors.

3.8.2 The Four Most Conductive Elements

Considering the four most conductive elements, silver oxide (Ag_2O) is a black conductor with resistivity around $3 \times 10^{-3}\ \Omega \cdot cm$ [81]. This is higher than that of silver metal by over 3 orders of magnitude.

Cuprous oxide (Cu_2O) is a red to brown p-type semiconductor with a temperature dependent resistivity. The resistivity also depends on the method of formation, but a range of $25\ \Omega \cdot cm$ to $10^4\ \Omega \cdot cm$ is representative [82]. Suffice to say that copper oxide resistivity is greater than that of metallic copper by a factor exceeding at least a million. Thin films might have relatively low resistance through the thickness, but this cannot be relied upon as conductors age or corrode.

Gold does not tarnish in response to oxygen or ordinary environmental contaminants.

Aluminum is an excellent electrical conductor and is routinely used in many

applications where proper attention to joint implementation is observed. However, aluminum oxide (Al_2O_3) is an excellent insulator, and forms on the metal surface more or less immediately upon exposure to air. It reaches a thickness $\approx 1.5\ nm$ in a few hours. Growth of thickness continues as the logarithm of exposure time [83].

On one hand, the resistivity of aluminum oxide is generally quoted as $> 10^{14}$ $\Omega \cdot cm$. This means that a 1 cm^2 layer 1.5 nm thick still presents a formidable 15 megohms of resistance. On the other hand, the dielectric strength, though an impressive 16.7 kV/mm (nominal), equates to a breakdown of only 25 *millivolts* across the same thickness. Distances of this order of magnitude also allow the possibility of electron tunneling. Suffice to say that the interstrand properties of paralleled aluminum conductors that are only loosely packed against each other lack definitive rules.

3.8.3 Inter-strand Currents

Strand-to-strand currents will not flow between points of contact where voltages are equal. Theoretically identical adjacent strands carrying equal currents will lack an inter-strand potential difference at any point along the distributed voltage drop of the wire. Real conductors have slight differences along their lengths, but the resulting potential differences and associated interstrand currents are commensurately small. Some or all of the mentioned effects may be found in stranded conductors, making them to some degree a low cost substitute for litz wire [84].

Proximity effect in the conductor bundle will cause current differentials at sufficiently high frequencies. If high conductive intimacy is present, it allows the strand bundle to act as if it were electrically solid, supporting eddy currents more or less comparable to solid wire, albeit with many small air channels in the cross

section.

This discussion has deliberately pursued a maximal argument for independence of adjacent conductors. Casual experimentation with a length of stranded wire and an ohmmeter may readily suggest otherwise. The best available counsel is probably "caveat emptor" unless the specifics of a material choice and conductor implementation are known.

3.9 Stranded Shields

There are two fundamental theoretical models for coaxial shields. Solid shields are well understood but their rigidity limits their sphere of application. Stranded shields are an important resource for the design of flexible cables. Single layer stranded shields are discussed here, inasmuch as they are popular and are foundational for more complex constructions that include multiple braid layers, conductive foil, etc.

There are various ways to create a single layer shield from wire strands. A simple, inexpensive approach is a served shield, which applies a covering layer of strands in a lazy spiral around the dielectric surface. The spiraling keeps the shield conductors organized and coverage can be essentially 100%, but served shields buckle when flexed, and therefore are not reliably constant impedance. At higher frequencies, the spiraling causes inductive effects. Served shields are typically intended only to provide electrostatic shielding at low frequencies, such as the audio range. Hill and Wait [85] analyzed served design for deliberately leaky RF cables.

A strand layer may be applied in strictly axial fashion (no spiraling), which results in acceptable or even superior high frequency performance [86]. A tight wrap of material over the shield layer is necessary to maintain the shield against the

dielectric surface. This prevents strand migration during flexure and ensures constant impedance.

A common flexible shield construction uses tubular braid woven from flat groups of wire strands. Half of the weave spirals in a left-hand sense and half in a right-hand sense. This keeps the shield intimate with the dielectric during flexure. Non-zero strand thickness precludes complete closure of the weave at crossover points, resulting in interstices ("eyes") in the braid. The effect is usually described in terms of "optical coverage," meaning the fraction of the dielectric surface covered by strands. Single layer coverage can be as high as 98%. A typical value is 95%.

3.9.1 Modeling Single Braided Shields

Braided shield performance continues to be an unsettled topic. The parameters of concern are the degree of shielding between inner and outer environments and also between cables [87]. Both theoretical and empirical approaches have been tried with mixed results.

Braided shields are often modeled as hollow metallic tubes, with or without periodic apertures to represent the eyes. Vance modeled braided shields as perforated tubes [88], as did Lee and Baum [89]. Kley [90] compared a perforated tube model against cable samples with single-braided shields and stated:

> "The known approaches for the calculation of the coupling parameters of single-braided shields do not compare well against the measured values.",

and

> "...no significant dependence ...on the contact resistance between the braids could be stated."

Zhou and Gong [91] asserted that Schelkunoff's formulas for a cylindrical shell [92] were not applicable to cable braids, and derived an analytical model consistent with Vance's work but assuming braided shield construction.

Tyni proposed a twin inductance model for transfer impedance calculation based on braid inductance and leakage inductance [93]. He asserted that braid inductance results from the textile nature of the braid, while leakage inductance is caused by the eyes in the braid.

Tyni's parameters were:

α : Braid angle

Dm : Mean braid diameter

b : Hole width

d : Braid-wire diameter

h : Radial spindle separation

μ : Permeability

N : Number of folding

Kirschvink and Vroomen [94] stated:

> "The design of cable braids is still based on experience and experiments because a correct modelization of the transfer impedance is not showing correct results if all the construction parameters of a braid are taken into account."

Their parameter set was:

D : Diameter under braid

m : Number of foldings

n : Number of wires per folding

d : Diameter of the wires

h : Length of lay

Schippers et al [95] studied braid samples and compared their model against those of Vance and Kley. They asserted that a braided shield has six parameters:

D : Diameter of braid

C : Number of carriers (i.e. belts of wires)

N : Number of wires in a carrier

d : Diameter of a single wire

σ : Conductivity of the wires

α : Weave angle of the braid

Sali created a refined model for braided coaxial cables after comparing the work of Vance and Tyni to measurements of experimental cables [96]. He concluded:

> "These studies have confirmed that the agreement between the measured and the theoretical results were largely dependent on the braid designs. Tyni's approach has produced the highest accuracy for the leaky and overbraided cables but failed to produce any sensible agreement for cables with optimized braid designs."

Rahmann et al [97] combined Tyni's work with that of Vance to achieve a better fit to measured data. Xiaoling et al [98] studied the results from Tyni, Sali, and Kley, and set forth another model, stating:

> "The predictions of the existing approaches have excellent accuracy at low frequencies, but have poor accuracy at high frequencies."

Tiedemann and Gonschorek experimented with RG 213/U cables and discovered that hole coupling and braid porpoising effects are counteracting, corroborating the work of Vance and Rahmann et al. They achieved a 20 dB improvement in shielding by *removing* wires from the braid [99]. Cook and Wilson verified the "over-braiding" phenomena [100].

Badr et al compared wire braids with tape braids to better understand the mechanism of current conduction, and concluded that construction tolerances were critical [101]. Tiedemann experimented with current flow in the braided shields of commercial coaxial cables, and concluded that braid current follows individual conductor paths without substantive current sharing. He explicitly rejected the perforated tube model [102].

For other than gold or gold-plated braids, a more realistic model of braided shields seems to be one of interwoven, axially counter-wound, lazy pitch inductors with magnetic field cancellation as the basis of high frequency performance [103][104]. The slightly increased distance along the spiral paths ($\approx 5\%$) also implies a modest slow wave effect [105] similar to that mentioned for litz conductors. In fact, a larger implication is that braided shields may be a de facto litz derivative subject to similar considerations and optimization strategies.

3.10 Roughness Effects

Conductor roughness is not often considered in high frequency design. Industry standard insertion loss estimation techniques assume smooth surfaces [106]. However, standard printed circuit foils have roughnesses that can be significant at frequencies as low as the VHF region.

3.10.1 Surface Roughness

When skin depth becomes comparable to the magnitude of surface deviations the effective current path length approximately doubles with a commensurate increase in loss [107]. This is shown graphically in figure 3.7.

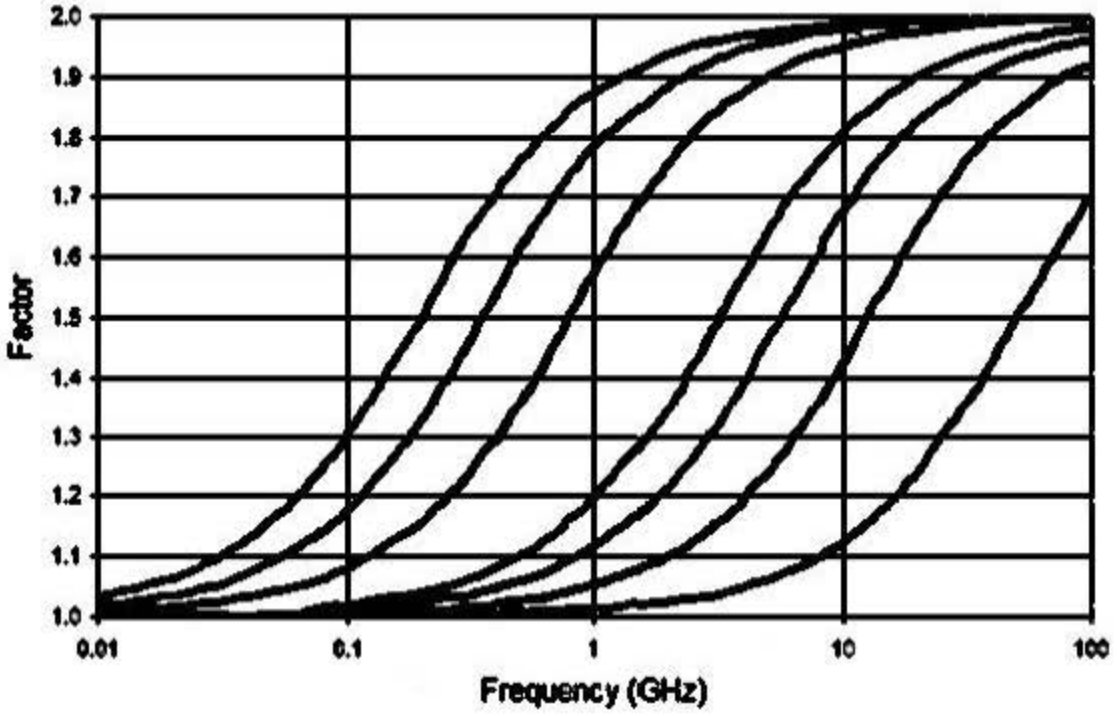

Figure 3.7: Loss factors for 4, 3, 2, 1, 0.75, 0.5, and 0.25 mils RMS roughness

An RMS surface roughness equivalent to one skin depth increases power loss by approximately 60% [108]. Dispersion also increases substantially in this region [109]. Beyond the obvious effect of surface roughness on inductance in this region, a related effect is an increase in capacitance contribution from the tips of the surface asperities. This effect was first noted for the case of thin insulating film [110] and later for the case of printed circuit laminate [111]. This makes the effective dielectric constant dependent upon strip width for thin dielectrics, in the same sense that roughness makes insertion loss dependent upon strip width. A practical methodology for measuring roughness effects to 50 GHz is discussed in [112].

3.10.2 Foil Surface Roughness

Printed circuit foils are commonly etched on one side to improve adhesion to the base laminate. Printed circuit based microstrip transmission lines concentrate the anti-parallel currents at the facing surfaces, precisely where the etching is applied. Although some loss reduction strategies buff the outward conductor faces and burnish via-hole interiors, these are the least efficacious places to apply it, with only limited potential for loss mitigation.

The flexibility of printed circuit processes make it possible to design buried microstrip that has smooth foil surfaces facing each other. The resulting microstrip will have reduced surface roughness losses but higher dielectric losses compared to surface implementation. There will also be less impedance control since the dielectric thickness between facing smooth foils will be created by manual insertion of prepreg[6] between the foil layers rather than the tightly controlled thickness of

[6] Prepreg is a layer of uncured epoxy-glass material that is manually inserted into the multilayer stack as a dielectric spacer. It becomes part of the finished board when the stack is cured in a heated press. Prepreg thickness might diminish somewhat in the process. Since the minimum thickness of a sheet of prepreg is that of a single layer of woven glass fibers, the final thickness has granularity of approximately that amount, typically around 3.5 mils.

prefabricated laminate.

In response to demand for higher electrical performance, some laminate vendors offer products with smoother inner surfaces, although users must accept somewhat reduced foil robustness against peeling [113]. Figure 3.8 shows cross sectional roughness examples for external (surface trace), internal trace, and smooth foils [114].

3.10.3 Foil Edge Roughness

The chemical etching processes typically used to create foil conductors interact with the grain structure of the copper with the result of an uneven edge. Etching also proceeds faster with increasing distance from the laminate surface. This creates a trapezoidal cross section that multiplies width uncertainty as a matter of geometry. Conductors etched from typical printed circuit foils have width roughness on the order of a thousandth of an inch.

Roughness amplitude is proportional to foil thickness and independent of conductor width. Narrower conductors are more vulnerable than wider ones. A trace only 0.004" wide with .001" uncertainty on each edge looks ragged under a microscope.

Similarly, the line edge roughness of metallization used in microelectronics is on the order of a few nanometers and does not decrease as devices shrink. For features below 45 nm, this can result in device parameter fluctuations and impose design limits [115]. Figure 3.9 shows representative roughness for a 45 nm process.

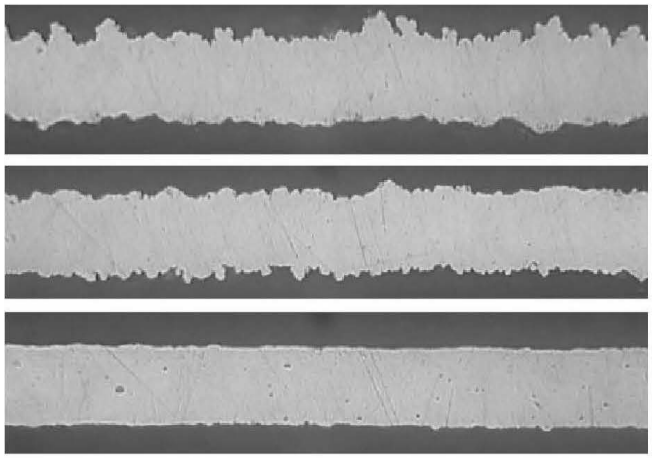

Figure 3.8: Top: surface trace, Middle: internal trace, Bottom: smooth foil

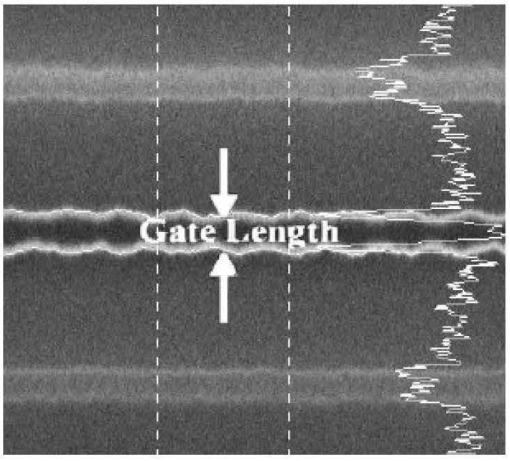

Figure 3.9: SEM image line edge roughness (Ban)

3.10.4 Roughness Modes

Edge roughness can be divided into two modes. The sum of the profiles of both edges divided by two is common mode roughness, while the difference divided by two represents differential mode roughness. Common mode roughness represents a conductor of average width wandering from side to side about the nominal center line. Differential mode roughness equals width deviations that represent impedance changes. Those of high spatial frequency compared to the wavelength of the signal are essentially invisible, while those that are comparable affect return loss.

If conductor width is comparable to skin depth or less, common and differential roughnesses are meaningful concepts. If the width is large compared to skin depth, current will be concentrated at the edges and each edge will act more or less independently. Thus, the entire roughness of each will contribute to high frequency losses. However, the edge contributions will be of less significance compared to the total conducting area.

Mechanical removal processes such as milling and routing or laser ablation[7] create foil edges that are more smooth and vertical than those of etching processes [116]. These are preferred when precise high frequency performance is wanted[8] .

[7] An example of a commercial laser ablation product is the LPKF Protolaser U3.

[8] "The center frequencies in the milled circuits were closer to the computer-predicted value, while those for ...etched circuits were a little higher. ... microscopic examination revealed deviations from exact design dimensions of +0.5 to +1.0 mil in the mechanically milled filter and +2.0 to +5.0 mil in the chemically etched version. The milled circuits ...provided a more precise mechanical match to the original filter-design pattern because their traces were square and sharp, just as they were defined by electromagnetic (EM) CAD images. The etching process produced softer, more rounded edges." (Schmidt)

CHAPTER 4

COMPARATIVE PERFORMANCE

For a fixed conductor cross sectional area, which shape of conductor is superior? The answer is the nearly universal, "It depends." The conductor choices compared in figure 4.1 are based on equal cross sectional area [11]. As frequency rises, obvious differences emerge. Thin wall tubular conductors exhibit the same characteristic shape as solid wire, which is simply the zero internal diameter limiting case. Although thin walled tubular conductors offer superior characteristics, at a sufficiently high frequency skin effect sets an upper bound for information capacity (e.g. bit rate), for any given conductor material and type of transmission line [117][118].

Rectangular and ribbonoid conductors likewise differ only in degree[1] . The contrasting response shapes between circular and rectangular conductors invariably cross over at sufficiently high frequency. Thus, planar conductor information capacity is limited by maximum tolerable attenuation rather than geometry per se. Above TEM cutoff, higher order modes can contribute to the usable spectrum for short pulse, fast risetime signals if certain effects are ignorable or controlled for [119].

The general characteristics of tubular and rectangular conductors govern the nominal performance of bimetallic, laminated, litz, or stranded constructions, although these cannot be compared directly because they depend on many additional parameters.

[1] The curve for a 16:1 aspect ratio strap is approximately that for a nominal 0.012" wide trace implemented in 1/2 oz. (0.0007" thick) foil, albeit without accounting for dielectric effects or proximity to other conductors.

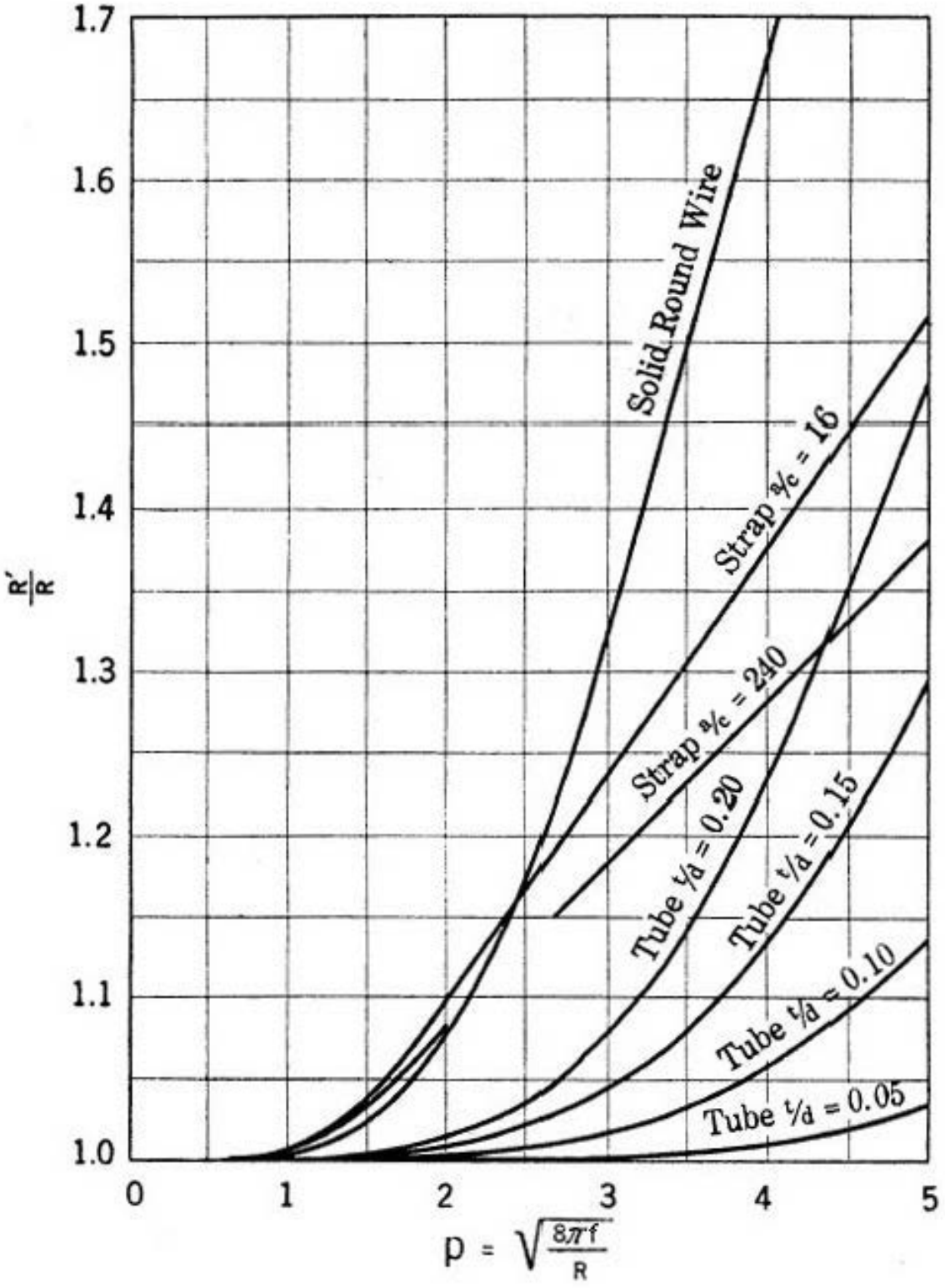

Figure 4.1: Resistance Ratio versus Root of Frequency Normalized by R

CHAPTER 5

CONCLUSIONS AND FUTURE WORK

Current flow in a conductor is shown to have both in-phase (real) and quadrature phase (reactive) components with associated counter flows. The consequent loss terms have characteristic spatial distances that allow loss minimization through choice of appropriate conductor dimensions. An important conclusion is that dimensional choices can be used to flatten frequency response with beneficial results for wideband signals.

Solid wire is indicated for low frequency applications because it is low cost and adequate. Solid wire is used for the center conductors of low cost transmission cables for applications where flatness and loss are of lesser concern.

Tubular or bimetallic conductors offer flatter response at low frequencies and lower loss at high frequencies. They are well suited for low loss transmission of signals of limited bandwidth (although that bandwidth can be considerable) such as cable television signals, or high frequency narrowband signals for which the change in slope across the bandwidth is negligible, such as radio and television broadcast.

Rectangular or square conductors are often specified for mechanical considerations, such as strength or packing density. In the instance of bulk power, such as for utilities, this choice also offers larger surface area for heat dissipation, and avoidance of dimensions that are excessive compared to skin depth.

The flatter, wider frequency response of ribbonoid conductors suggests that they are superior to circular geometries for fast rise time digital signaling and other wideband applications. They also offer compact, low cost form factors for

microwave transmission lines and high speed digital signaling.

Laminated conductors potentially offer very low loss coaxial cables, but have yet to attain commercial importance due to their complexity.

Litz wire offers low loss at modest RF frequencies, for instance to minimize eddy current losses in the copper of transformer or inductor windings.

Stranded wire is used primarily to offer mechanical flexibility and long service life. It may also offer litz-like characteristics.

It is noted that braided shield characteristics are rather more complex than basic analyses suggest.

The present work emphasizes the frequency domain. A future task is to further extend analyses in time domain terms. Extension to cylindrical and other form factors is already found in the literature, but the perspective of multiple current flows developed in chapter 2 should be further pursued for these contexts. Current metrics for surface and edge roughness effects are not well developed and can be further explored.

Thus far, experimental confirmation of conductor theory has been largely confined to exterior measurements. Direct experimental confirmation of conductor interior effects is possible and would be a contribution.

Given their importance, further inquiry into the physics of braided shields is still a fruitful area for investigation. Further investigation of laminated and litz conductor architectures may be productive as well.

BIBLIOGRAPHY

[1] D. K. Cheng, "Field and wave electromagnetics," *Addison Wesley Publishing Co.*, pp. 437–443, 1990.

[2] P. C. Magnusson, G. C. Alexander, V. K. Tripathi, and A. Weisshaar, "Transmission lines and wave propagation," *CRC Press*, pp. 78–82, 2001.

[3] E. Holzman, "Wideband measurement of the dielectric constant of an FR4 substrate using a parallel-coupled microstrip resonator," *Microwave Theory and Techniques, IEEE Transactions on*, vol. 54, no. 7, pp. 3127 – 3130, 2006.

[4] L. W. Ritchey, "A survey and tutorial of dielectric materials used in the manufacture of printed circuit boards," Speeding Edge, Tech. Rep., 1999.

[5] R. Mildner, "Developments in high-frequency transmitter cables," *Journal of the British Institution of Radio Engineers*, vol. 13, no. 2, pp. 113–121, 1953.

[6] A. Ducluzaux, "Extra losses caused in high current conductors by skin and proximity effects," Schneider Electric, Tech. Rep. Cahier Technique no. 83, 2002.

[7] H. A. Wheeler, "Formulas for the skin effect," *Proceedings of the I.R.E.*, vol. 30, no. 9, pp. 412–424, 1942.

[8] O. M. O. Gatous and J. Pissolato, "Frequency dependent skin effect formulation for resistance and internal inductance of a solid cylindrical conductor," *Microwaves, Antennas and Propagation, IEE Proceedings*, vol. 151, no. 3, pp. 212–216, 2004.

[9] C. Yen, Z. Fazarinc, and R. Wheeler, "Time domain skin effect model for transient analysis of lossy transmission lines," *Proceedings of the IEEE*, vol. 70, no. 7, pp. 750 – 757, 1982.

[10] K. W. Miller, "Diffusion of electric current into rods, tubes, and flat surfaces," *American Institute of Electrical Engineers, Transactions of the*, vol. 66, no. 1, pp. 1496–1502, 1947.

[11] H. B. Dwight, "Skin effect in tubular and flat conductors," *American Institute of Electrical Engineers, Transactions of the*, vol. XXXVII, no. 2, pp. 1379–1403, 1918.

[12] Robin Materials Inc., "Invar," http://rmat.com/invar.html.

[13] G. Odam, "Status of draft stanags 4236 and 4327," in *Edition 2*, no. Technical Paper 1999-01-2391. SAE International, 1999, Structural Lightning Safety, Section 5.1.6 see 1.5 Magnetic Pressure and Forces.

[14] V. A. Rakov and F. Rachidi, "Overview of recent progress in lightning research and lightning protection," *Electromagnetic Compatibility, IEEE Transactions on*, vol. 51, no. 3, pp. 428–442, 2009.

[15] A. Arnold, "Proximity effect in solid and hollow round conductors," *Electrical Engineers, Journal of the Institution of, Part II: Power Engineering*, vol. 88, no. 4, pp. 349–359, 1941.

[16] G. S. Smith, "Proximity effect in systems of parallel conductors," *Journal of Applied Physics*, vol. 43, no. 5, pp. 2196–2203, 1972.

[17] W. G. Hurley, E. Grath, and J. G. Breslin, "Optimizing the AC resistance of multilayer transformer windings with arbitrary current waveforms," *Power Electronics, IEEE Transactions on*, vol. 15, no. 2, pp. 369–376, 2000.

[18] S. W. Stratton, "Circular of the Bureau of Standards no. 31 copper wire tables," Bureau of Standards (NIST), Tech. Rep., 1914.

[19] "Conductivity and resistivity values for iron and alloys," Collaboration for NDT Education, Tech. Rep., 2002.

[20] R. A. Matula, "Electrical resistivity of copper, gold, palladium, and silver," *Journal of Physical Chemistry Reference Data*, vol. 8, no. 4, p. 1161, 1979.

[21] J. R. Davis, "Copper and copper alloys," *ASM Specialty Handbook*, 2001.

[22] "ASTM B682 - 01(2009) standard specification for standard metric sizes of electrical conductors," ASTM International, Tech. Rep., 2009.

[23] "Copper-clad aluminum (CCA) indoor wiring solutions guide," Commscope Inc., Tech. Rep. BB-SO-BM-1, 2012.

[24] "Copper clad grounding solutions guide for utility applications," Commscope Inc., Tech. Rep., 2011.

[25] "ASTM B452 - 09 standard specification for copper-clad steel wire for electronic application," ASTM International, Tech. Rep., 2009.

[26] US Department of Defense, "MIL-DTL-17H detail specification, cables, radio frequency, flexible and semirigid, general specification for," Downloadable from http://www.everyspec.com, 2005, supercedes MIL-C-17G (1990).

[27] "ASTM B869 - 07(2013) standard specification for copper-clad steel electrical conductor for CATV drop wire," ASTM International, Tech. Rep., 2013.

[28] AMP Incorporated, "Golden rules: Guidelines for the use of gold on connector contacts," Tyco Electronics Corporation, Tech. Rep., 2004.

[29] R. Schueller and C. Hillman, "Understanding the risk of gold flash," DfRSolutions, Tech. Rep., 2010.

[30] M. Ferguson and C. Fieselman, "Manufacturing concerns when soldering with gold plated component leads or circuit board pads," *Components, Packaging, and Manufacturing Technology, Part C, IEEE Transactions on*, vol. 20, no. 3, pp. 188–193, 1997.

[31] Y. Shlepnev and S. McMorrow, "Nickel characterization for interconnect analysis," in *Electromagnetic Compatibility (EMC), 2011 IEEE International Symposium on*, 2011, pp. 524–529.

[32] J. Wilkerson, P. Lam, K. Gard, and M. Steer, "Distributed passive intermodulation distortion on transmission lines," *Microwave Theory and Techniques, IEEE Transactions on*, vol. 59, no. 5, pp. 1190 – 1205, 2011.

[33] A. Bhatia, "Electrical conductors, course no: E02-005," Continuing Education and Development, Inc. (cedengineering.com), Tech. Rep., 2006.

[34] J. Miller, "Effective resistance and inductance of iron and bimetallic wires," *Bulletin of the Bureau of Standards*, vol. 12, pp. 207–267, 1915, NIST Research Library.

[35] B. Teare and J. Webb, "Skin effect in bimetallic conductors," *American Institute of Electrical Engineers, Transactions of the*, vol. 62, no. 6, pp. 297–302, 1943.

[36] B. Fei, M. Fei, and Z. Chen, "High electric conduction property of composite copper-clad steel wire," *Electromagnetic Compatibility, IEEE Transactions on*, vol. 41, no. 3, pp. 196–201, 1999.

[37] Y. Yoon, J. Park, and M. Allen, "Polymer-core conductor approaches for RF MEMS," *Microelectromechanical Systems, Journal of*, vol. 14, no. 5, pp. 886 – 894, 2005.

[38] J. M. Eglin, "U.S. patent 1972877 concentric return transmission system," 1934.

[39] V. N. Ostreiko, "Calculating the radii of a tubular conductor with electrically optimal wall thickness," *Russian Electrical Engineering*, vol. 70, no. 10, pp. 65–66, 1999.

[40] J. Carson, "U.S. patent 1817964 concentric conductor transmission system," 1931.

[41] A. Arnold, "The alternating current resistance of tubular conductors," *Electrical Engineers, Journal of the Institution of*, vol. 78, no. 473, pp. 580–596, 1936.

[42] O. Coufal, "Current density in a pair of solid coaxial conductors," *Electromagnetics*, vol. 27, pp. 299–320, 2007.

[43] E. Post, "Phase, attenuation, and impedance characteristics of coaxial transmission lines with thin tubular conductors," *Microwave Theory and Techniques, IEEE Transactions on*, vol. 11, no. 2, pp. 129–136, 1963.

[44] M. D. Fanton, "Transmission line for broadcast applications," *ERI Technical Series*, vol. 6, 2006.

[45] J. Bryant, "Coaxial transmission lines, related two-conductor transmission lines, connectors, and components: A U.S. historical perspective," *Microwave Theory and Techniques, IEEE Transactions on*, vol. 32, no. 9, pp. 970 – 981, 1984.

[46] H. B. Dwight, "Reactance and skin effect of concentric tubular conductors," *American Institute of Electrical Engineers, Transactions of the*, vol. 61, no. 7, pp. 513–518, 1942.

[47] A. Clogston, "Reduction of skin effect loss by the use of laminated conductors," *Bell System Technical Journal*, vol. 30, no. 3, pp. 491–529, 1951.

[48] H. S. Black, C. O. Mallinckrodt, and S. P. Morgan-Jr., "Experimental verification of the theory of laminated conductors," *Proceedings of the IRE*, vol. 40, no. 8, pp. 902–905, 1952.

[49] J. A. Brandao Faria, "A matrix approach for the evaluation of the internal impedance of multilayered cylindrical structures," *Progress In Electromagnetics Research B*, vol. 28, pp. 351–367, 2011.

[50] A. Kurs, M. Kesler, and S. Johnson, "Optimized design of a low resistance electrical conductor for the multimegahertz range," *Applied Physics Letters*, vol. 98, no. 17, pp. 1–4, 2011.

[51] J. M. Manley, "A three conductor elementary clogston coaxial transmission line - calculation, fabrication and experiment," *Bell System Technical Journal*, vol. 42, no. 6, pp. 2551–2574, 1963.

[52] Y. Iwashita, H. Fujisawa, M. Ichikawa, and Y. Tajima, "Reduction of RF skin loss with thin foils," in *Particle Accelerator Conference, 2007. PAC. IEEE, Proceedings of*, 2007, pp. 2134–2136.

[53] E. F. Vaage, "Transmission properties of laminated Clogston type conductors," *Bell System Technical Journal*, vol. 32, no. 3, pp. 695–713, 1953.

[54] H. Ataka, "A series laminated conductor for high frequencies," *Proceedings of the IRE*, vol. 42, no. 10, pp. 1527 – 1529, 1954.

[55] F. Medina and R. Marques, "Comments on "internal impedance of conductors of rectangular cross-section"," *Microwave Theory and Techniques, IEEE Transactions on*, vol. 49, no. 8, pp. 1511–1513, 2001.

[56] G. Antonini, A. Orlandi, and C. Paul, "Internal impedance of conductors of rectangular cross-section," *Microwave Theory and Techniques, IEEE Transactions on*, vol. 47, no. 7, pp. 979–985, 1999.

[57] ——, "Author's reply," *Microwave Theory and Techniques, IEEE Transactions on*, vol. 49, no. 8, pp. 1512–1513, 2001.

[58] Y. Shlepnev, "Modeling frequency dependent conductor loss and dispersion in serial data channel interconnects," pdf, Simberian Inc., Tech. Rep., 2007. [Online]. Available: www.simberian.com

[59] Y. Shlepnev and C. Nwachukwu, "Roughness characterization for interconnect analysis," in *Electromagnetic Compatibility (EMC), 2011 IEEE International Symposium on*, 2011, pp. 518–523 see table 1.

[60] W. Heinrich, "Comments on "internal impedance of conductors of rectangular cross-section"," *Microwave Theory and Techniques, IEEE Transactions on*, vol. 49, no. 3, pp. 580–581, 2001.

[61] H. Kim and C. C. P. Chen, "Be careful of self and mutual inductance formulae," http://ccf.ee.ntu.edu.tw/~cchen/research/CompInduct9.pdf, Tech. Rep., 2009.

[62] Z. Piatek and B. Baron, "Exact closed form formula for self inductance of conductor of rectangular cross-section," *Progress In Electromagnetics Research M*, vol. 26, pp. 225–236, 2012.

[63] W. Weeks, L. L. Wu, M. F. McAllister, and A. Singh, "Resistive and inductive skin effect in rectangular conductors," *IBM Journal of Research and Development*, vol. 23, no. 6, pp. 652–660, 1979.

[64] H. Chen and J. Fang, "Modeling of impedance of rectangular cross-section conductors," in *Electrical Performance of Electronic Packaging, 2000, IEEE Conference on.*, 2000, pp. 159–162.

[65] P. Silvester, "AC resistance and reactance of isolated rectangular conductors," *Power Apparatus and Systems, IEEE Transactions on*, vol. PAS-86, no. 6, pp. 770–774, 1967.

[66] P. Waldow and I. Wolff, "The skin-effect at high frequencies," *Microwave Theory and Techniques, IEEE Transactions on*, vol. 33, no. 10, pp. 1076–1082, 1985.

[67] C. Hoer and C. Love, "Exact inductance equations for rectangular conductors with applications to more complicated geometries," *Journal of Research of the National Bureau of Standards - C*, vol. 69C, no. 2, pp. 127–137, 1965.

[68] A. Ruehli, "Inductance calculations in a complex integrated circuit environment," *IBM Journal of Research and Development*, vol. 16, no. 5, pp. 470 – 481, 1972.

[69] G. Zhong, "Exact closed-form formula for partial mutual inductances of rectangular conductors," *Circuits and Systems I: Fundamental Theory and Applications, IEEE Transactions on*, vol. 50, no. 10, pp. 1349 – 1352, 2003.

[70] M. P. Perry, "Low frequency electromagnetic design," *CRC Press*, pp. 103–106, 1985.

[71] A. Reatti and F. Grasso, "Solid and litz wire winding non-linear resistance comparison," in *Circuits and Systems, 2000. Proceedings of the 43rd IEEE Midwest Symposium on*, vol. 1, 2000, pp. 466–469.

[72] C. R. Sullivan, "Optimal choice for number of strands in a litz wire transformer winding," *Power Electronics, IEEE Transactions on*, vol. 14, no. 2, pp. 283–291, 1999.

[73] J. A. Ferreira, "Analytical computation of AC resistance of round and rectangular litz wire windings," *Electric Power Applications, IEE Proceedings B*, vol. 139, no. 1, pp. 21–25, 1992.

[74] H. Rossmanith, M. Doebroenti, M. Albach, and D. Exner, "Measurement and characterization of high frequency loss in nonideal litz wires," *Power Electronics, IEEE Transactions on*, vol. 26, no. 11, pp. 3386–3394, 2011.

[75] J. Pollock, T. Abdallah, and C. R. Sullivan, "Easy to use CAD tools for litz wire winding optimization," in *Applied Power Electronics Conference and Exposition, 2003. APEC '03. Eighteenth Annual IEEE*, vol. 2, 2003, pp. 1157–1163.

[76] R. Beekman, "NEMA magnet wire thermal class ratings," Essex Group, Inc., Tech. Rep., 2004.

[77] H. B. Dwight, "Skin effect and proximity effect in tubular conductors," *American Institute of Electrical Engineers, Transactions of the*, vol. XLI, pp. 189–198, 1922.

[78] J. Kim, E. Song, J. Cho, Y. Shiim, G. Kim, and J. Kim, "Frequency dependent transmission line model of a stranded coaxial cable," *EICE Transactions on Electronics*, vol. E93-C, no. 1, pp. 112–119, 2010.

[79] M. Kashani, "Frequency dependent resistance calculation of stranded conductors in transmission lines by an exponential formula based on the subdivision technique," Master's thesis, University of British Columbia, 1993.

[80] X. Tang and C. R. Sullivan, "Stranded wire with uninsulated strands as a low cost alternative to litz wire," in *Power Electronics Specialist Conference, 2003. PESC '03. 2003 IEEE 34th Annual*, vol. 1, 2003, pp. 289–295.

[81] S. Uthanna, M. H. P. Reddy, P. Boulet, C. Petitjean, and J. F. Pierson, "Effect of deposition temperature on the physical properties of RF magnetron sputtered Ag-Cu-O films with various Cu to Ag ratios," *Physica Status Solidi*, vol. 207, no. 7, pp. 1655 – 1659, 2010.

[82] V. Drobny and L. Pulfrey, "Properties of reactively-sputtered copper oxide thin films," *Thin Solid Films*, vol. 61, no. 1, pp. 89 – 98, 1979.

[83] J. Boggio and R. Plumb, "Theory of formation of very thin oxide films on metals," *Chemical Physics, Journal of*, vol. 44, pp. 1081–1086, 1966.

[84] X. Tang and C. R. Sullivan, "Optimization of stranded wire windings and comparison with litz wire on the basis of cost and loss," in *Power Electronics Specialists Conference, 2004. PESC 04. 2004 IEEE 35th Annual*, vol. 2, 2004, pp. 854–860.

[85] D. A. Hill and J. R. Wait, "Propagation along a coaxial cable with a helical shield," *Microwave Theory and Techniques, IEEE Transactions on*, vol. 28, no. 2, pp. 84–89, 1980.

[86] C. Nixon, "U.S. patent 4408089 extremely low attenuation extremely low radiation loss flexible coaxial cable for microwave energy in the gigahertz frequency range," 1983.

[87] C. R. Paul, "Transmission line modeling of shielded wires for crosstalk prediction," *Electromagnetic Compatibility, IEEE Transactions on*, vol. EMC-23, no. 4, pp. 345–351, 1981.

[88] E. F. Vance, "Shielding effectiveness of braided wire shields," *Electromagnetic Compatibility, IEEE Transactions on*, vol. EMC-17, no. 2, pp. 71–77, 1975.

[89] K. S. H. Lee and C. E. Baum, "Application of modal analysis to braided-shield cables," *Electromagnetic Compatibility, IEEE Transactions on*, vol. 17, no. 3, pp. 159–169, 1975.

[90] T. Kley, "Optimized single braided cable shields," *Electromagnetic Compatibility, IEEE Transactions on*, vol. 35, no. 1, pp. 1–9, 1993.

[91] G. Zhou and L. Gong, "An improved analytical model for braided cable shields," *Electromagnetic Compatibility, IEEE Transactions on*, vol. 32, no. 2, pp. 161–163, 1990.

[92] S. A. Schelkunoff, "The electromagnetic theory of coaxial transmission lines and cylindrical shields," *Bell System Technical Journal*, vol. 13, no. 4, pp. 532–579, 1934.

[93] M. Tyni, "Transfer impedance of coaxial cables with braided outer conductors," in *Research Proceedings of Wroclaw Institute of Telecommunications and Akusticcs*, 1975, pp. 410–419.

[94] M. Kirschvink and P. Vroomen, "Optimal cable screening braids determined by a computer-aided statistical planning method," in *Electromagnetic Compatibility, 1994. Symposium Record. Compatibility in the Loop., IEEE International Symposium on*, 1994, pp. 31–36.

[95] H. Schippers, J. Verpoorte, and R. Otin, "Electromagnetic analysis of metal braids," in *Proc. of the 10th Int. Symposium on Electromagnetic Compatibility (EMC Europe 2011)*, York, U.K., September 2011, pp. 543–548.

[96] S. Sali, "An improved model for the transfer impedance calculations of braided coaxial cables," *Electromagnetic Compatibility, IEEE Transactions on*, vol. 32, no. 2, pp. 139–143, 1991.

[97] M. Rahmann, B. Sitch, and F. Benson, "Leakage from coaxial cables," *Physical Science, Measurement and Instrumentation, Management and Education - Reviews, IEE Proceedings A*, vol. 127, no. 2, pp. 74–80, 980.

[98] W. Xiaoling, L. Chao, D. Hao, and W. Lixin, "An improved model for the transfer impedance calculations of braided coaxial cables," in *Power Electronics and Motion Control Conference (IPEMC), 2012 7th International*, vol. 2, 2012, pp. 1078–1081.

[99] R. Tiedemann and K. H. Gonschorek, "Minimizing the interference coupling into standard coaxial cables with braided shield," in *Electromagnetic Compatibility, 1998 IEEE International Symposium on*, vol. 1, 1998, pp. 501–504.

[100] C. J. Cook and D. Wilson, "Investigation and analysis of the over-braid phenomena in flexible coaxial cables," *56th International Wire & Cable Symposium, Proceedings of the*, pp. 431–435, 2007.

[101] A. Badr, F. Benson, and M. Rahman, "Current conduction in coaxial cable cables at radio frequencies," *Physical Science, Measurement and Instrumentation, Management and Education - Reviews, IEE Proceedings A*, vol. 128, no. 5, pp. 354–357, 1981.

[102] R. Tiedemann, "Current flow in coaxial braided shields," *Electromagnetic Compatibility, IEEE Transactions on*, vol. 45, no. 3, pp. 531–537, 2003.

[103] J. R. Wait, "Electromagnetic theory of the loosely braided coaxial cable: Part I," *Microwave Theory and Techniques, IEEE Transactions on*, vol. 24, no. 9, pp. 547–553, 1976.

[104] D. R. Hill and J. R. Wait, "Electromagnetic theory of the loosely braided coaxial cable: Part II numerical results," *Microwave Theory and Techniques, IEEE Transactions on*, vol. 28, no. 4, pp. 326–331, 1980.

[105] P. Madle, "Contact resistance and porpoising effects in braid shielded cables," in *Proceedings of the 1980 IEEE International Symposium on Electromagnetic Compatibility*, 1980, pp. 206–210.

[106] S. Hinaga, M. Y. Koledintseva, P. K. R. Anmula, and J. L. Drewniak, "Effect of conductor surface roughness upon measured loss and extracted values of PCB laminate material dissipation factor," in *Proceedings of the Technical Conference*, 2009.

[107] Polar Staff, "Surface roughness effect on PCB trace attenuation/ loss," Polar Instruments, Tech. Rep. Application Note AP8155, 2011.

[108] S. P. Morgan Jr., "Effect of surface roughness on eddy current losses at microwave frequencies," *Journal of Applied Physics*, vol. 20, no. 4, pp. 352–362, 1949.

[109] A. Horn III, J. W. Reynolds, P. A. LaFrance, and J. C. Rautio, "Effect of conductor profile on the insertion loss, phase constant, and dispersion in thin high frequency transmission lines," in *DesignCon 2010*, 2010.

[110] G. Palasantzas and J. De Hosson, "The effect of mound roughness on the electrical capacitance of a thin insulating film," *Solid State Communications*, vol. 118, pp. 203–206, 2001.

[111] A. Deutsch, A. Huber, G. V. Kopcsay, B. J. Rubin, R. Hemedinge, D. Care, W. Becke, T. Winkel, and B. Chamberlin, "Accuracy of dielectric constant measurement using the full-sheet-resonance technique IPC-TM-650 2.5.5.6," in *Electrical Performance of Electronic Packaging, 2002*, 2002, pp. 311–314.

[112] Y. Shlepnev and C. Nwachukwu, "Practical methodology for analyzing the effect of conductor roughness on signal losses and dispersion in interconnects," in *DesignCon 2012*, 2012.

[113] Rogers, "Copper foils for high frequency materials," Rogers Corporation, Tech. Rep. 92-243, 2011.

[114] T. Liang, M. Hudson, S. Hall, H. Heck, and G. Brist, "A practical method for modeling PCB transmission lines with conductor surface roughness and wideband dielectric properties," in *Microwave Symposium Digest, 2006. IEEE MTT-S International*, 2006, pp. 1780–1783.

[115] Y. Ban, S. Sundareswaran, R. Panda, and D. Pan, "Electrical impact of line-edge roughness on sub-45nm node standard cell," in *Proc. SPIE 7275, Design for Manufacturability through Design-Process Integration III*, 2009.

[116] S. Schmidt, "Compact router speeds prototype PCB development," *Microwaves & RF Magazine*, pp. 115–116, 118, January 2001.

[117] D. Miller and H. Ozaktas, "Limit to the bit-rate capacity of electrical interconnects from the aspect ratio of the system architecture," *Journal of Parallel and Distributed Computing*, vol. 41, no. 1, pp. 42–52, 1997.

[118] R. Sarvari, "Impact of size effects and anomalous skin effect on metallic wires as GSI interconnects," Ph.D. dissertation, Georgia Institute of Technology, 2008.

[119] J. Barth and J. Richner, "Distortion of fast pulses by non-TEM effects in coaxial cables," in *Proceedings of the Second International Conference on Ultra-Wideband, Short Pulse Electromagnetics*, L. Carin and L. Felsen, Eds., vol. Ultra-Wideband, Short-Pulse Electromagnetics 2, 1995, pp. 305–312.

[120] "Magnet wire / winding wire engineering data handbook," Essex Group Inc., www.superioressex.com, Tech. Rep., 2009.

[121] "MWS tech book," MWS Wire Industries, Tech. Rep., 2011.

APPENDIX A

CURRENT FLOW IN A CONDUCTIVE HALF-SPACE

Let $J_z(x) = J_0 e^{\frac{-x}{\delta}} \cos(\omega t - \frac{x}{\delta})$ (starting assumption)

$= J_0 e^{\frac{-x}{\delta}} \left(\cos(\omega t)\cos\left(\frac{x}{\delta}\right) + \sin(\omega t)\sin\left(\frac{x}{\delta}\right)\right)$ (apply identity)

$= J_0 e^{\frac{-x}{\delta}} \left(\cos(\omega t)\ \text{"real part"} + \sin(\omega t)\ \text{"reactive part"}\right)$

Let $\frac{x}{\delta} = \xi$. Then, $I_z(\xi) = \int_0^\infty J_z(\xi) d\xi$

$= J_0 \cos(\omega t) \int_0^\infty e^{-\xi} \cos(\xi)\, d\xi + J_0 \sin(\omega t) \int_0^\infty e^{-\xi} \sin(\xi)\, d\xi$

$= \frac{1}{2} J_0 e^{-\xi} \left[\cos(\omega t)(\sin\xi - \cos\xi) - \sin(\omega t)(\sin\xi + \cos\xi)\right]\Big|_0^\infty$

$= \frac{1}{2} J_0 (\cos\omega t + \sin\omega t)$ *amps/meter* (summary result)

The summary result is recalculated in terms of individual components. Each is the sum of all regions of similar flow. Let $I_Z = I_F + I_R + I_L + I_C$, where:

I_F = sum of forward real currents: $\cos\xi > 0$

I_R = sum of reverse real currents: $\cos(\xi) < 0$

I_L = sum of inductive currents: $\sin(\xi) > 0$

I_C = sum of capacitive currents: $\sin(\xi) < 0$

$I_F = J_0 \cos(\omega t) \left[\int_0^{\frac{\pi}{2}} e^{-\xi}\cos\xi d\xi + \sum_{n=0}^{\infty}\left(\int_{\frac{\pi}{2}(4n+3)}^{\frac{\pi}{2}(4n+5)} e^{-\xi}\cos\xi d\xi\right)\right]$

$\int_0^{\frac{\pi}{2}} e^{-\xi}\cos\xi d\xi = \frac{1}{2}\left(e^{-\xi}(\sin\xi - \cos\xi)\right)\Big|_0^{\frac{\pi}{2}} = \frac{1}{2}\left(e^{-\frac{\pi}{2}} + 1\right) = 0.603\,94$

$\sum_{n=0}^{\infty}\left(\int_{\frac{\pi}{2}(4n+3)}^{\frac{\pi}{2}(4n+5)} e^{-\xi}\cos(\xi)\, d\xi\right) = \frac{1}{2}\sum_{n=0}^{\infty}\left(e^{-\xi}(\sin\xi - \cos\xi)\Big|_{\frac{\pi}{2}(4n+3)}^{\frac{\pi}{2}(4n+5)}\right)$

$= \frac{1}{2}\sum_{n=0}^{\infty}\left(e^{-\frac{\pi}{2}(4n+5)} + e^{-\frac{\pi}{2}(4n+3)}\right) = \frac{1}{2}\sum_{n=0}^{\infty} e^{-\frac{\pi}{2}(2n+3)} = \frac{1}{2}\frac{e^{2\pi}}{e^{\frac{7}{2}\pi} - e^{\frac{5}{2}\pi}} = 0.004\,69$

$I_F = (0.603\,94 + 0.004\,69)\, J_0 \cos(\omega t) = 0.608\,63 J_0 \cos(\omega t)$

The first term contributes $\frac{0.60394}{0.60863} = 99.23\%$ of I_F.

$$I_R = J_0 \cos(\omega t) \left(\sum_{n=0}^{\infty} \int_{\frac{\pi}{2}(4n+1)}^{\frac{\pi}{2}(4n+3)} e^{-\xi} \cos(\xi)\, d\xi \right)$$
$$= \tfrac{1}{2} J_0 \cos(\omega t) \sum_{n=0}^{\infty} \left(e^{-\xi} (\sin\xi - \cos\xi) \Big|_{\frac{\pi}{2}(4n+1)}^{\frac{\pi}{2}(4n+3)} \right)$$
$$= -\tfrac{1}{2} J_0 \cos(\omega t) \sum_{n=0}^{\infty} \left(e^{-\frac{\pi}{2}(4n+3)} + e^{-\frac{\pi}{2}(4n+1)} \right) = -\tfrac{1}{2} J_0 \cos(\omega t) \sum_{n=0}^{\infty} e^{-\frac{\pi}{2}(2n+1)}$$
$$= -\tfrac{1}{2} \frac{e^{2\pi}}{e^{\frac{5}{2}\pi} - e^{\frac{3}{2}\pi}} = -0.108\,63 J_0 \cos(\omega t)$$

$$I_{REAL} = I_F + I_R = (0.608\,63 - 0.108\,63)\, J_0 \cos(\omega t) = \tfrac{1}{2} J_0 \cos(\omega t)$$

$$I_L = J_0 \sin(\omega t) \left(\sum_{n=0}^{\infty} \int_{\pi 2n}^{\pi(2n+1)} e^{-\xi} \sin(\xi)\, d\xi \right)$$
$$= -\tfrac{1}{2} J_0 \sin(\omega t) \left(\sum_{n=0}^{\infty} e^{-\xi} (\sin\xi + \cos\xi) \Big|_{\pi 2n}^{\pi(2n+1)} \right)$$
$$= \tfrac{1}{2} J_0 \sin(\omega t) \sum_{n=0}^{\infty} \left(e^{-\pi(2n+1)} + e^{-\pi 2n} \right) = \tfrac{1}{2} J_0 \sin(\omega t) \sum_{n=0}^{\infty} e^{-\pi n}$$
$$= \tfrac{1}{2} J_0 \sin(\omega t) \frac{e^{2\pi}}{e^{2\pi} - e^{\pi}} = 0.522\,583 J_0 \sin(\omega t)$$

$$I_C = J_0 \sin(\omega t) \left(\sum_{n=0}^{\infty} \int_{\pi(2n+1)}^{\pi(2n+2)} e^{-\xi} \sin(\xi)\, d\xi \right)$$
$$= -\tfrac{1}{2} J_0 \sin(\omega t) \left(\sum_{n=0}^{\infty} e^{-\xi} (\sin\xi + \cos\xi) \Big|_{\pi(2n+1)}^{\pi(2n+2)} \right)$$
$$= -\tfrac{1}{2} J_0 \sin(\omega t) \sum_{n=0}^{\infty} \left(e^{-\pi(2n+2)} + e^{-\pi(2n+1)} \right) = -\tfrac{1}{2} J_0 \sin(\omega t) \sum_{n=0}^{\infty} e^{-\pi(n+1)}$$
$$= -\tfrac{1}{2} J_0 \sin(\omega t) \frac{e^{2\pi}}{e^{3\pi} - e^{2\pi}} = -0.02\,258\,3 J_0 \sin(\omega t)$$

$$I_{REACTIVE} = I_L + I_C = (0.522\,583 - 0.02\,258\,3)\, J_0 \sin(\omega t) = \tfrac{1}{2} J_0 \sin(\omega t)$$

Net total current (that which an instantaneous reading ammeter would indicate) is

$$I_Z = I_{REAL} + I_{REACTIVE} = \tfrac{1}{2} J_0 (\cos(\omega t) + \sin(\omega t))$$

This is the same as the summary result.

APPENDIX B

TABLE OF SELECT COPPER WIRE ATTRIBUTES

This table is based on modern data for electrical grade copper (i.e. not the IACS constants published in 1913). The resistivity of annealed, high purity copper electrical wire is $\approx 1.678 * 10^{-8}\ \Omega \cdot m$ (102.75% IACS, 20° C). The density of soft-drawn, annealed copper wire is ≈ 8924 kg/m^3 (20° C).

Table entries are for single, round, bare wires in isolation. The presence of insulation will increase kg/km.

Transition frequency is calculated by setting $radius = \delta$. This is the demarcation point between low frequency conduction and higher frequencies where skin effect becomes significant.

Note that excessive tension will cause wire elongation. Example tensioning guidelines are found in [120][121].

Table B.1: Select Copper Wire Attributes

AWG	D inch	D mm	mm2	kg/km	Ω/km	Ftrans
4/0	0.460000	11.68	1.072E+02	9.569E+02	1.565E-01	1.25E+02
3/0	0.409642	10.40	8.503E+01	7.588E+02	1.973E-01	1.57E+02
2/0	0.364797	9.266	6.743E+01	6.018E+02	2.488E-01	1.98E+02
1/0	0.324861	8.251	5.348E+01	4.772E+02	3.138E-01	2.50E+02
1	0.289297	7.348	4.241E+01	3.785E+02	3.957E-01	3.15E+02
2	0.257626	6.544	3.363E+01	3.001E+02	4.989E-01	3.97E+02
3	0.229423	5.827	2.667E+01	2.380E+02	6.292E-01	5.01E+02
4	0.204307	5.189	2.115E+01	1.888E+02	7.934E-01	6.31E+02
5	0.181941	4.621	1.677E+01	1.497E+02	1.000E+00	7.96E+02
6	0.162023	4.115	1.330E+01	1.187E+02	1.261E+00	1.00E+03
7	0.144285	3.665	1.055E+01	9.414E+01	1.591E+00	1.27E+03
8	0.128490	3.264	8.366E+00	7.466E+01	2.006E+00	1.60E+03
9	0.114424	2.906	6.634E+00	5.921E+01	2.529E+00	2.01E+03
10	0.101897	2.588	5.261E+00	4.695E+01	3.189E+00	2.54E+03
11	0.090742	2.305	4.172E+00	3.723E+01	4.022E+00	3.20E+03
12	0.080808	2.053	3.309E+00	2.953E+01	5.071E+00	4.04E+03
13	0.071962	1.828	2.624E+00	2.342E+01	6.395E+00	5.09E+03
14	0.064084	1.628	2.081E+00	1.857E+01	8.064E+00	6.42E+03
15	0.057068	1.450	1.650E+00	1.473E+01	1.017E+01	8.09E+03
16	0.050821	1.291	1.309E+00	1.168E+01	1.282E+01	1.02E+04
17	0.045257	1.150	1.038E+00	9.262E+00	1.617E+01	1.29E+04
18	0.040303	1.024	8.231E-01	7.345E+00	2.039E+01	1.62E+04
19	0.035891	0.9116	6.527E-01	5.825E+00	2.571E+01	2.05E+04
20	0.031961	0.8118	5.176E-01	4.619E+00	3.242E+01	2.58E+04
21	0.028462	0.7229	4.105E-01	3.663E+00	4.088E+01	3.25E+04
22	0.025347	0.6438	3.255E-01	2.905E+00	5.154E+01	4.10E+04
23	0.022572	0.5733	2.582E-01	2.304E+00	6.500E+01	5.17E+04
24	0.020101	0.5106	2.047E-01	1.827E+00	8.196E+01	6.52E+04
25	0.017900	0.4547	1.624E-01	1.449E+00	1.034E+02	8.22E+04
26	0.015941	0.4049	1.288E-01	1.149E+00	1.303E+02	1.04E+05
27	0.014196	0.3606	1.021E-01	9.113E-01	1.643E+02	1.31E+05
28	0.012641	0.3211	8.097E-02	7.226E-01	2.072E+02	1.65E+05
29	0.011258	0.2860	6.422E-02	5.731E-01	2.613E+02	2.08E+05
30	0.010025	0.2546	5.092E-02	4.545E-01	3.295E+02	2.62E+05
31	0.008928	0.2268	4.039E-02	3.604E-01	4.155E+02	3.31E+05
32	0.007950	0.2019	3.203E-02	2.858E-01	5.240E+02	4.17E+05
33	0.007080	0.1798	2.540E-02	2.267E-01	6.606E+02	5.26E+05
34	0.006305	0.1601	2.014E-02	1.798E-01	8.330E+02	6.63E+05
35	0.005615	0.1426	1.598E-02	1.426E-01	1.050E+03	8.36E+05
36	0.005000	0.1270	1.267E-02	1.130E-01	1.325E+03	1.05E+06
37	0.004453	0.1131	1.005E-02	8.967E-02	1.670E+03	1.33E+06
38	0.003965	0.1007	7.966E-03	7.109E-02	2.106E+03	1.68E+06
39	0.003531	0.08969	6.318E-03	5.638E-02	2.656E+03	2.11E+06
40	0.003145	0.07988	5.012E-03	4.473E-02	3.348E+03	2.66E+06

APPENDIX C

ECONOMICS OF COPPER WIRE MANUFACTURING

Of many styles of copper wire that differ mostly in insulation details, magnet wire was chosen for study because the simple film insulation system is a minor cost adder. Magnet wire is also an important commodity product whose price is kept close to marginal cost by market forces. Thus, market pricing for this product category closely reflects the economics for production of the wire itself.

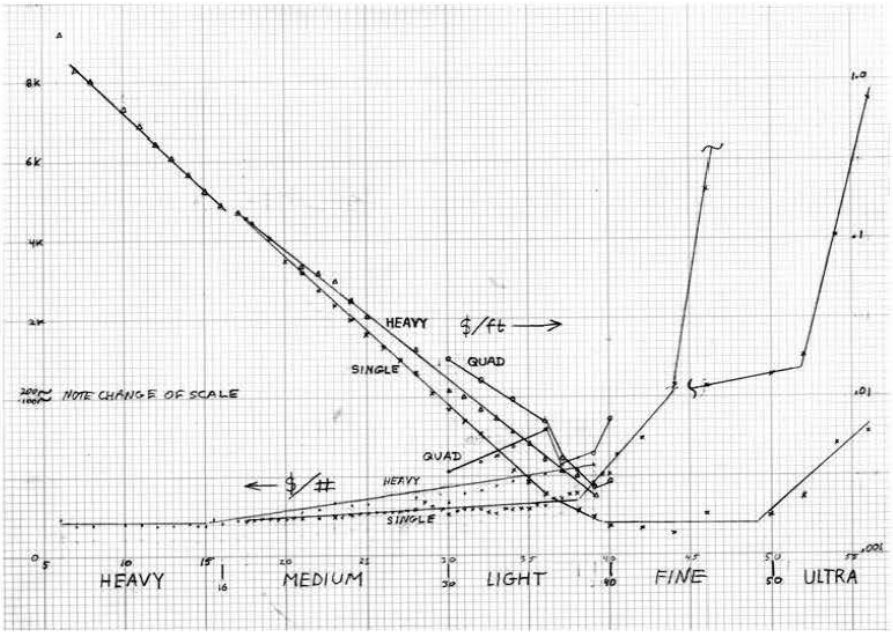

Figure C.1: Magnet Wire Cost per Pound and per Foot (2008 market data)

2008 market pricing for commercial magnet wire shows distinct cost regions versus wire gauge. The data predates later disruptions of the copper wire market caused by heavy demand for copper products of all kinds and abrupt price

fluctuations for the raw material.

7/0 to 16 AWG: Cost per unit weight is nearly constant. Purchase of wire in these gauges amounts to sale of bulk copper, the only difference being the diameter and length per pound for each gauge in this range. Only "heavy" (double) insulation is offered, which is needed to withstand the mechanical forces associated with winding thick, stiff conductors. The heaviest gauges are often purchased in stranded form (not charted here) for reasons of mechanical flexibility. In addition to round wire, square and rectangular form factors are readily available (not charted here).

16-30 medium gauge: Single and heavy insulation weights are available, with a modest cost slope for each. Cost per unit length continues to drop, but cost per unit weight begins to rise slightly as insulation costs increase. The most popular sizes of general purpose wire are in this region.

30-36 light gauge: Cost per unit length continues downward. Single insulated wire continues the upward cost per pound trend, but heavy insulation assumes a steeper slope. Triple and quad insulations are available with commensurate cost increases.

36-40 transition to fine gauges: The cost per unit length for single insulated wire assumes a more modest slope. There is a mild kink in the cost per unit weight curve for heavy insulation. Quad insulated wire has a distinct low cost dip associated with popular gauges for high turn count, high voltage windings. The cost per unit weight for single insulation begins a fast rise.

40-48 fine wire: Copper cost is essentially irrelevant compared to processing, therefore cost per unit length is relatively constant in this region. Cost per pound is therefore proportional to feet per pound and rises aggressively. Heavy and quad insulation are not offered from stock.

48 – 52 extra fine: Cost per foot begins to rise aggressively, and cost per pound skyrockets.

52 -60 ultra fine: The cost skyrocket enters the stratosphere, reaching $8,000 per pound for AWG 56. This is low demand specialty wire that is truly difficult to manufacture. Pull lengths are extraordinary and the wire is exceedingly delicate and easily broken. Production handling requires finger cots for protection from corrosive skin oils, and microscopes and tweezers are essential tools. Insulation becomes an increasing fraction of winding volume and weight.

54 gauge (859,100 feet per pound, bare) and 56 gauge (1,366,000 feet per pound, bare) conductors are offered in spools not exceeding .25 and .156 pounds respectively. This is more than 40 miles (64 km) of wire in each instance.

APPENDIX D

STRANDED WIRE CONSTRUCTION

There are four concentric stranded constructions offered by wire and cable manufacturers. Manufacturers also offer low cost bunched stranding and high-strand-count rope stranding.

The industry normally refers to "Concentric" as "True Concentric" and uses the terms interchangeably. Concentric or True Concentric is characterized by a central wire surrounded by one or more layers of helically laid wires in a geometric pattern, with alternately reversed lay direction and increasing lay length.

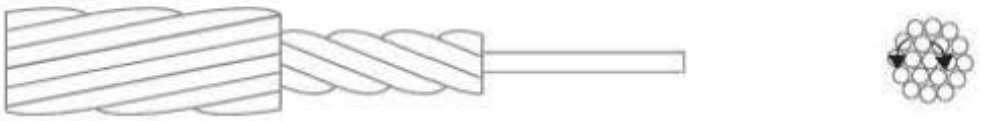

Figure D.1: Concentric Stranding

Equilay or Equilay Concentric is characterized by a central wire surrounded by one or more layers of helically laid wires in a geometric pattern, with alternately reversed lay direction and the same lay length.

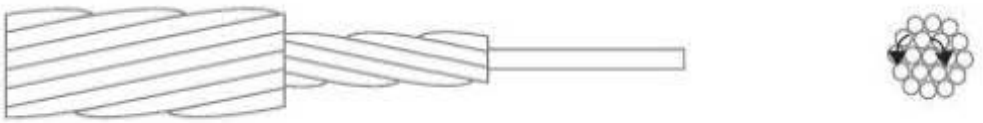

Figure D.2: Equilay Stranding

Unidirectional or Unidirectional Concentric is characterized by a central wire surrounded by one or more layers of helically laid wires in a geometric pattern, with the same lay direction and an increasing lay length.

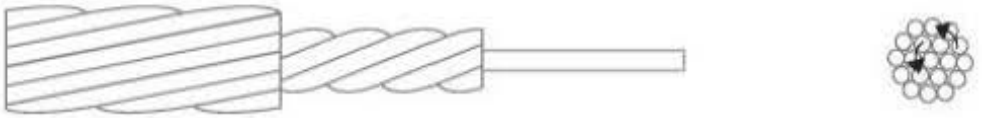

Figure D.3: Unidirectional Stranding

Unilay or Unidirectional Equilay Concentric stranding is characterized by a central wire surrounded by one or more layers of helically laid wires in a geometric pattern, with the same lay direction and the same lay length. This is the only concentric construction in which strand layers remain in parallel contact throughout the length of the conductor.

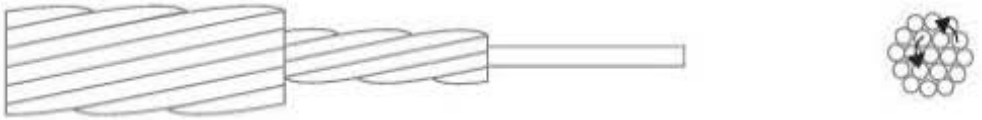

Figure D.4: Unilay Stranding

Bunched Stranding parallels any number of strands in a random pattern and twists them in one operation, giving all strands the same lay direction and lay length. The result is a rougher surface and lower dimensional tolerance than concentric constructions. The number of strands is determined by the size of the individual strands and the total cross-sectional area required.

Figure D.5: Bunched Stranding

Rope construction consists of concentric or bunched members stranded together into the final concentric or bunched configuration. Rope stranding has the advantage of increased mechanical flexibility through use of a larger number of finer strands while offering tighter diameter tolerance than a simple bunched construction. Ropes are more common for larger diameters, but applications often require the flexibility of rope construction in smaller sizes. Constructions vary and may contain hundreds or thousands of strands.

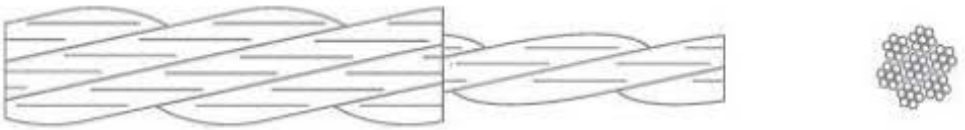

Figure D.6: Rope Stranding

Figures and information courtesy of Calmont Wire, Santa Ana, CA, USA.

APPENDIX E

COPYRIGHTS AND PERMISSIONS

Tables: Laney 2013 (CC BY-NC-ND 3.0)

Figures: as shown

Figure	Author	Year	Status
2.1	Yen et al	1982	© IEEE
2.2	Laney	2013	(CC BY-NC-ND 3.0)
2.3	Ducluzaux	2002	Extracted Schneider Cahier Technique no. 83
3.1	Hurley et al	2000	© IEEE
3.2	Fei et al	1999	© IEEE
3.3	Miller	1915	public domain (issued by U.S. gov't agency)
3.4	Eglin	1934	public domain (issued by U.S. gov't agency)
3.5	Clogston	1951	© IEEE
3.6	Ducluzaux	2002	Extracted Schneider Cahier Technique no. 83
3.7	Polar staff	2011	used by permission
3.8	Liang et al	2006	© IEEE
3.9	Ban et al	2009	SPIE (CC BY 3.0)
4.1	Dwight	1918	© expired
App. C	Laney	2013	(CC BY-NC-ND 3.0)
App. D	Calmont	——	used by permission